Journal of Energy Storage 125 (2025) 117043

Contents lists available at ScienceDirect

Journal of Energy Storage

journal homepage: www.elsevier.com/locate/est

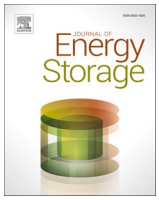

Research papers

Numerical analysis of cold thermal energy storage systems using macro-encapsulated Phase Change Materials (PCM) in residential cooling applications

M. Caliano [a,*], N. Bianco [b], G. Graditi [a], L. Mongibello [a]

[a] ENEA – Agenzia Nazionale per le Nuove Tecnologie, l'Energia e lo Sviluppo Economico Sostenibile, P.le E. Fermi, 1, 80055 Portici, NA, Italy
[b] Dipartimento di Ingegneria Industriale (DII), Università di Napoli Federico II, P.le V. Tecchio 80, Napoli 80125, Italy

ARTICLE INFO

Keywords:
Cold thermal energy storage (TES)
Macro-encapsulated phase change materials (PCM)
Residential cooling applications
Numerical and experimental analysis
Energy storage efficiency
COMSOL Multiphysics and MATLAB modeling

ABSTRACT

The study focuses on the numerical simulation of the charging and discharging phases of a thermal energy storage designed for cold applications, utilizing water and a macro-encapsulated Phase Change Material (PCM). The experimental setup, used for the experimental validation, comprises an electric chiller, a heat exchanger, and a 320-liter cold storage tank containing 55 aluminum bottles filled partially with a biological PCM. This setup experimentally simulates a residential scenario in Italy's climate zone E, characterized by minimum winter temperatures below 0 °C and maximum summer temperatures over 25 °C. Numerical simulations are performed through the commercial solver COMSOL Multiphysics integrated with Matlab. A one-dimensional Matlab model simulates water behavior in the storage tank, while the performance of the PCM is analyzed using the Effective Heat Capacity (EHC) method in COMSOL Multiphysics. Key results include system charging/discharging times, water temperature variation, energy storage charge/discharge rates, and the PCM melt fraction. The numerical data on water temperature variations inside the tank are compared with experimental results, showing good agreement. Additionally, a parametric analysis is performed to assess how the size of the PCM container influences the system's performance.

1. Introduction

1.1. Background

Phase Change Materials (PCMs) are substances renowned for their high thermal energy storage density, since they rely on high latent heat for thermal energy storage, typically from solid to liquid and vice versa for thermal energy release. This characteristic makes PCMs ideal for managing temperature fluctuations and conserving energy [1,2].

PCMs have versatile applications across various fields [3,4]. In building construction, they regulate indoor temperatures by absorbing excess heat during the day and releasing it when temperatures fall. This process reduces the need for artificial heating and cooling, enhancing comfort, saving energy, and improving building efficiency [5,6]. In solar energy storage, PCMs store heat generated from solar collectors, releasing it when sunlight is not available. This ensures a consistent supply of thermal energy, even during periods of low solar irradiance, supporting the effective use of renewable energy and contributing to sustainability [7,8].

Thermal management systems also benefit from PCMs, which provide solutions for temperature regulation in technological and industrial processes. For instance, in electronic devices, PCMs help manage heat dissipation, protecting sensitive components from overheating and extending their lifespan [9,10]. In cold storage applications, PCM-based systems maintain temperature consistency. PCM packs in refrigeration units can provide cooling during power outages or reduce cooling energy requirements, which is especially valuable in sectors like pharmaceuticals where precise temperature control is crucial [11].

PCMs enhance temperature control in cold storage and HVAC systems, offering significant benefits in energy efficiency, cost savings, and grid stability [12–14]. By integrating PCMs into HVAC systems, cooling energy can be stored during off-peak hours, such as at night, and released during high-demand periods [15,16]. This process, known as peak shaving, reduces strain on electrical grids during peak times and minimizes the need for additional cooling power, leading to operational cost savings. Additionally, PCMs improve HVAC efficiency, particularly

* Corresponding author.
E-mail address: martina.caliano@enea.it (M. Caliano).

https://doi.org/10.1016/j.est.2025.117043
Received 3 December 2024; Received in revised form 30 April 2025; Accepted 10 May 2025
Available online 13 May 2025

in regions with high cooling demands, by mitigating peak load impacts. This improves grid stability, reduces the risk of overloading, and lowers overall energy consumption, which can decrease greenhouse gas emissions from electricity generation. Thus, PCMs contribute to sustainability by enhancing the efficiency of existing systems without solely relying on increased energy supply.

1.2. Literature review

Many authors have conducted experiments on phase change materials for both hot and cold TES. They have also developed various models to simulate the phase change process.

Charvát et al. [17] investigated the use of paraffin-based PCMs in a solar air-based thermal system. Their research aimed to optimize the thermal performance of solar collectors by integrating paraffin PCMs, which are known for their stable and predictable phase change properties. The study demonstrated that paraffin-based PCMs could effectively improve the thermal storage capacity of solar air systems, leading to enhanced performance and reliability of solar heating applications. Allouhi et al. [18] focused on the numerical simulation of PCM melting and solidification processes within a solar collector. By employing advanced numerical methods, their study provided valuable insights into the dynamic behavior of PCMs during thermal cycles. Their findings highlighted the impact of PCM properties on the overall efficiency of solar collectors and emphasized the importance of accurate modeling for optimizing collector design and operation. Zhao et al. [19] examined various operational strategies for solar heating systems incorporating PCM-based thermal energy storage tanks. Their analysis included different charging and discharging strategies to maximize energy storage and retrieval efficiency. The study underscored the role of operational strategies in enhancing the performance of PCM-based TES systems and provided practical recommendations for system design and management. Bejarano et al. [20] conducted numerical studies on an innovative cold energy storage system that utilized PCMs. Their research introduced novel PCM formulations and system configurations aimed at improving the performance of cold storage applications. The study's outcomes demonstrated that careful selection and optimization of PCM properties could significantly enhance the efficiency of cold thermal energy storage systems. Cheng and Zhai [21] performed both numerical and experimental investigations on a cold thermal energy storage system that featured a packed bed with multiple PCMs. Their comprehensive study combined experimental data with numerical simulations to analyze the thermal performance of the multi-PCM system. The research provided valuable insights into the thermal behavior of packed beds with multiple PCMs, highlighting their potential for improving cold storage applications. Raul et al. [22] developed a mathematical model for latent heat thermal energy storage using encapsulated PCM. The study analyzed transient heat transfer fluid temperatures during charging and discharging, with experiments on a spherical capsule revealing the PCM's melting and solidification behavior. Farid et al. [23] utilized the Effective Heat Capacity (EHC) method to simulate 2D heat transfer involving phase change. The EHC method, known for its efficiency in handling phase change phenomena, was applied to model the thermal behavior of PCMs in various configurations. The study demonstrated the advantages of the EHC method in capturing the complex thermal dynamics of PCMs, contributing to more accurate and efficient simulations. Lamberg et al. [24] employed both the enthalpy method and the effective heat capacity method to simulate the melting and solidification processes of PCMs. By comparing these two approaches, their research highlighted the strengths and limitations of each method in different scenarios. The study provided a detailed analysis of the effectiveness of each simulation method, offering guidance on choosing the appropriate approach for specific PCM applications.

Encapsulating PCMs is essential for efficient thermal energy storage. It prevents leakage during phase changes, enhances thermal conductivity, and protects the material from environmental damage. Encapsulation also improves durability, maintains shape, and allows better integration with other materials, making PCMs more reliable and versatile in practical applications [25]. Many authors have considered encapsulated PCMs for enhance thermal performance of TES systems. Barba and Spiga [26] conducted research to evaluate the configuration of PCM encapsulation and analyzed the discharge performance of three geometric shapes of PCM—plates, cylinders, and spheres—within a sensible thermal energy storage (TES) tank. Their analysis covered aspects such as the time-dependent position of the solidification front, temperature profiles, the volume of solidified PCM, energy release, total solidification duration, and the influence of geometry and Jacob number on the final solidification time. They concluded that using small spherical capsules provided the most efficient setup, especially in scenarios requiring quick discharge. A similar investigation was performed by Al-Yasiri and Szabó [27], focusing on the thermal efficiency of concrete bricks containing PCM that was macro-encapsulated using aluminum containers. Their findings highlighted that the surface area of the encapsulation plays a critical role in governing the thermal response of the PCM, assuming all capsules have identical mass and placement. Ismail and Moraes [28] explored the solidification behavior of various PCMs encapsulated in both cylindrical and spherical forms of varying dimensions, using both computational and experimental approaches. Each configuration was subjected to the same surface temperature, with the objective of identifying an effective PCM-container combination suitable for use alongside refrigeration systems. In another experimental effort, Moreone et al. [29] used rectangular PCM slabs within a storage tank and demonstrated that the tank's energy storage potential increased by approximately 35 % in comparison to an identical tank filled solely with water. Heinz and Moser [30] contributed further with a study focusing on TES systems containing non-spherical macro-encapsulated PCMs. This research included numerical modeling that closely aligned with experimental outcomes. Their test setup featured a TES tank containing both PCM and a heat transfer fluid (HTF). The same methodology was adopted in our work. It was found that the inclusion of PCM enhanced the tank's storage capacity by roughly 14.5 % compared to a tank filled only with water. Rehman et al. [31] evaluated the thermal performance and practicality of cylindrical and rectangular PCM macro-encapsulation designs in thermal energy storage systems. They tested two configurations: one with equal PCM mass and another with maximum possible PCM mass. Using a salt hydrate with a 17 °C melting point, the experimental setup measures charging/discharging times, temperature profiles, heat transfer, and energy storage rates. Results highlight how geometry influences performance and support the optimization of encapsulation designs for improved efficiency and broader application in energy systems.

1.3. Contribution of the work

The study numerically investigates the charging and discharging dynamics of a TES system designed for cold applications. This system features water combined with a macro-encapsulated PCM. The setup for the experimental validation includes an electric chiller, a heat exchanger, and a 320-l cold storage tank filled with 55 aluminum bottles partially containing biological PCM. To experimentally simulate real thermal loads, a residential scenario typical of a single-family house in Italy's climate zone E is considered.

A one-dimensional finite difference Matlab model simulates water behavior within the storage tank, while COMSOL Multiphysics assesses PCM performance using the EHC method. The study evaluates various parameters, including system charging and discharging times, water temperature ranges, energy storage and discharge rates, and PCM melt fractions. Colorimetric maps illustrate temperature distributions and melt fractions at critical moments: the start and end of the cycle, along with two other significant time points.

As concerns the experimental validation, numerical simulations of

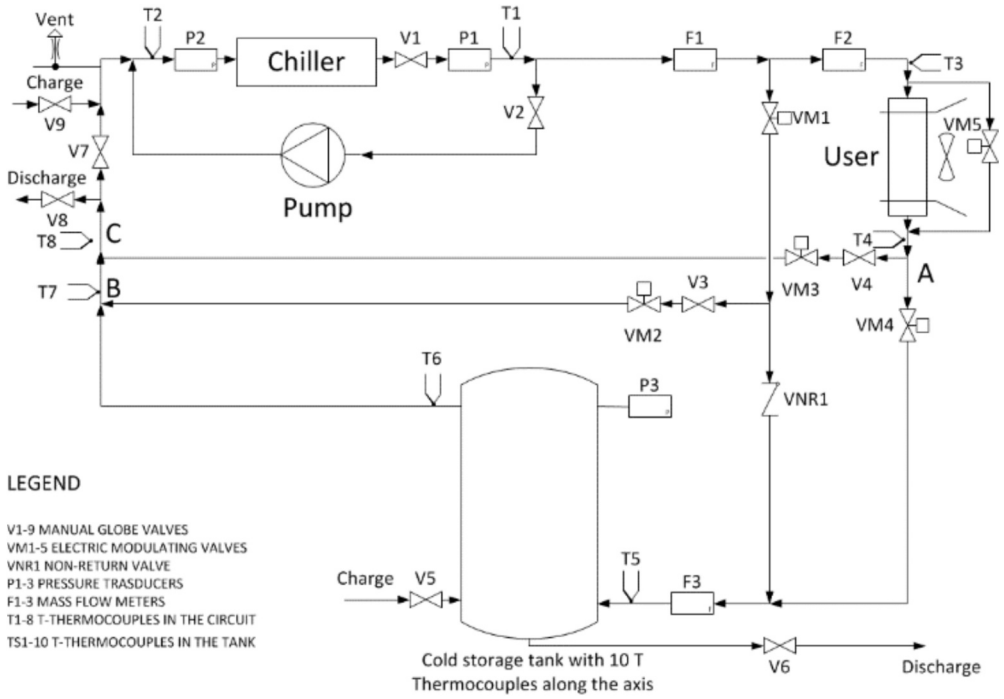

Fig. 1. Configuration of the cold storage test facility.

water temperature trends in the tank are compared with experimental data, showing a good match.

A numerical parametric analysis was performed to evaluate the energy performance of the water-cold storage system by varying the number and size of PCM containers. This analysis aimed to identify the best configuration of PCM container size and quantity to improve the system's thermal exchange performance for the specific case study. To facilitate this, the previously developed simulation application was updated to accommodate various storage system configurations, enabling a thorough comparison of different setups.

The analysis was based on a baseline scenario involving 1-l PCM bottles, experimentally studied at the ENEA Portici Research Center, which served as a benchmark for evaluating other configurations.

Four additional scenarios were numerically considered, each using different commercial sizes of PCM bottles: ½-liter, ¼-liter, 1/10-liter, and 1/636.6-liter. These scenarios were designed to examine how variations in bottle size affect the thermal performance of the cold storage system.

Simulations for these scenarios were conducted over 48 h with a results visualization time step of 100 s, while the baseline scenario was simulated for 72 h to allow for a more comprehensive evaluation of thermal equilibrium. The study included a detailed analysis of various factors such as water temperature trends, PCM temperature and melting fractions, and the energy stored and released by the PCM modules.

By examining these factors across different scenarios, the study aims to provide valuable insights into how the size and configuration of PCM bottles impact the overall efficiency of cold storage systems. The results are expected to guide the design and optimization of these systems, leading to improved energy performance and operational effectiveness.

Despite increasing interest in TES systems, particularly for cold applications, several critical areas remain underexplored. This study addresses specific gaps in current literature and practice, particularly concerning the use of macro-encapsulated PCMs in water-based cold storage systems. The following points summarize the main research gaps that motivate this investigation:

Fig. 2. Facility for the experimental analysis of cold storage systems at CR Enea Portici.

Fig. 3. Heat exchangers used to simulate refrigeration loads.

- Limited research on TES systems for cold applications utilizing water combined with macro-encapsulated PCM, particularly in residential settings.
- Scarcity of experimental-numerical hybrid studies that assess the dynamic thermal performance of cold storage systems under realistic residential thermal loads.
- Lack of comparative analyses regarding the impact of PCM container size and number on system efficiency and heat exchange performance.

To address the identified gaps and contribute to the optimization of TES systems for cold applications, this study establishes a set of targeted research objectives. The key objectives of the study are as follows:

- Investigate the charging/discharging dynamics of a TES system with macro-encapsulated PCM for cold storage applications.
- Develop and validate numerical models (using COMSOL Multiphysics and MATLAB) to simulate system behavior.
- Compare different PCM container configurations (sizes and quantities) to determine their influence on heat exchange efficiency and energy performance.
- Identify the optimal PCM configuration to enhance thermal storage performance.
- Visualize and analyze temperature profiles and melt fractions at critical time points to gain insights into thermal behavior across scenarios.

2. Setup and testing of experiments

Figs. 1 and 2 show the layout and a picture of the experimental facility at the ENEA Portici Research Center, respectively. The system consists of an electric vapor compression chiller, a heat exchanger that simulates refrigeration loads, and a cold storage tank. Temperature is measured using Type T thermocouples (Class 1) with an accuracy of ±0.5 °C, while flow is measured with Comac Flow 38 mass flow meters, which are accurate to 0.2 % of the measured value, down to 0.05 l/s.

The chiller, represented by the commercial chiller Thermo Scientific NESLAB ThermoFlex 24,000, shown in the lower part of Fig. 2, controls process fluid temperatures ranging from 5 °C to 40 °C and provides a maximum cooling power of 15 kW at 50 Hz with an outlet temperature of 5 °C. It operates effectively within ambient temperatures of 10 °C to 40 °C and includes a pump capable of delivering a maximum pressure head of approximately 4 bar at 50 Hz, maintaining process fluid temperature to within ±0.1 °C. Fig. 3 shows the Alfa Laval Optigo finned-tube heat exchangers used for simulating air conditioning thermal loads. These heat exchangers feature copper tubes, aluminum fins, and a total heat exchange area of 63.5 m^2, each with two fans (100 W each) with speed controlled by an inverter. They can transfer up to 25 kW of thermal power to the heat transfer fluid.

Figs. 4 and 5 show, respectively, the diagram and a photo of the 320-l cylindrical tank used for cold storage with water and macro-encapsulated PCM as the storage medium.

The tank is equipped with thermal insulation consisting of a 5 cm layer of polyurethane foam on its external walls. It features 9 thermocouples (type T, class 1) for measuring the water temperature along the tank's axis and a flange at the bottom for inserting the PCM bottles. Additionally, the tank includes a double-helix coil heat exchanger with a diameter of 1 in. and a surface area of 4 m^2, though this was not used in experimental simulations. During the experiments, the heat transfer fluid (demineralized water) enters the tank directly through one of the fittings at the bottom and exits through the outlet at the top. The tests were conducted with an empty coil, meaning the coil's volume of approximately 20 l did not contribute to the effective storage volume.

Fig. 6 displays one of the aluminum bottles used to contain the PCM, which has a melting temperature of 15 °C whereas Table 1 presents the thermophysical properties of the PCM [32]. It can be observed that the density of the PCM is lower than that of water; therefore, steel spheres were added to the bottles to ensure they remain at the bottom of the tank.

All experimental data have been recorded with a time-step of 1 s, using the National Instruments modules NI 9213 and NI 9208 for temperature and mass flow rate measurements, respectively, and the NI cRIO 9066 controller.

2.1. User characteristics

The user was chosen to model real thermal loads rather than scaled-down versions. For this, a single-family house with a useful floor area of 150 m^2, a shape factor of 0.9 m^{-1}, and located in climate zone E was selected for experimental refrigeration load simulation. The climatic zone E is characterized by cold winters with temperatures below 0 °C and frequent snow, cool summers with temperatures around 20–25 °C; it presents frequent precipitation (rain and snow), and high temperature variation between summer and winter. The annual thermal demand and daily profiles of electrical and thermal loads for summer air conditioning were calculated based on Mongibello et al. [33]. These calculations assumed that summer air conditioning, limited to June, July, and August, is provided by an electric vapor compression chiller with a hydronic system. The annual thermal demand for summer conditioning was set at 21 kWh/m^2/year, with identical hourly profiles for thermal and electrical loads used for all operating days. Fig. 7 shows the hourly averaged thermal and electrical load profiles for summer air conditioning on a standard summer day. The electrical load profile was constructed based on the chiller's Energy Efficiency Ratio (EER) as a function of ambient temperature. Fig. 8 illustrates the variation in the chiller's EER with the hourly average ambient temperature during the standard day. Both the hourly average ambient temperature and EER

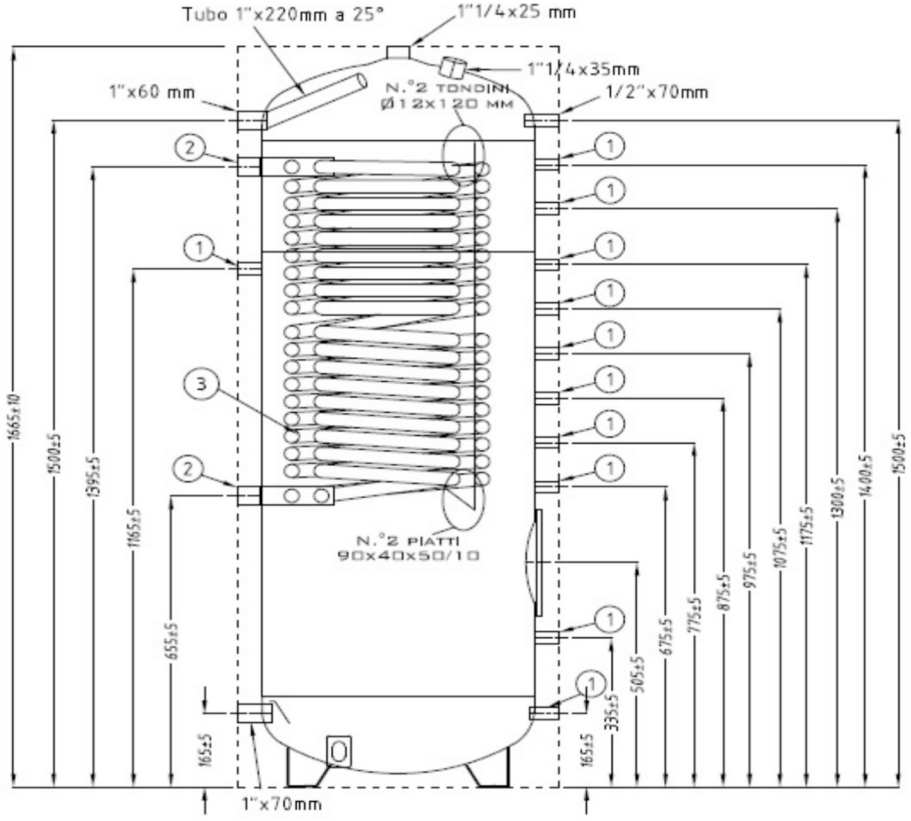

Fig. 4. Sketch diagram of the tank.

values in this figure were normalized to a maximum average temperature of 28 °C and a maximum EER of 3, respectively.

2.2. Design of the chiller and of the PCM-based cold storage, and experimental results

The sizing of the components of a cooling system with integrated cold storage cannot ignore the way in which the production of cold and its storage are managed. With reference to the loads shown in Fig. 9, it is clear that, without a cold storage system, and for a fixed set-point value of the comfort temperature inside the home, the operation of the chiller cannot be continuous during the hours characterized by a refrigeration load that is lower than the minimum cooling power that the chiller can deliver. During those hours, the air conditioning system controller would implement several stops and restarts, which negatively affect the performance and useful life of the system components. In fact, during those hours the controller would stop the chiller whenever the internal temperature reaches a predetermined set-point value. In light of this, to limit the number of stops and restarts and the nominal power of the chiller, the preliminary sizing of the chiller and the calculation of the capacity of the cold storage systems were carried out considering a "partial" cold storage, and based on the following assumptions on the operation of the chiller:

- the chiller, during its operation, must work at constant power, constant heat transfer fluid flow rate, and constant outlet temperature;
- the ratio between the cooling power transferred to the user and the cooling power supplied by the chiller must be greater than or equal to a predetermined minimum value, otherwise the chiller stops;
- the chiller cannot supply only the storage system, that is, the cold can be accumulated only in the periods in which the chiller must supply cooling power to the user.

The first of the above assumptions implies that the inlet temperature of the heat transfer fluid to the chiller must also be constant. The assumptions uniquely determine the nominal power of the chiller and the capacity of the cold storage system, for the user considered. Fig. 9 shows on the same graph the thermal power supplied by the chiller and the thermal loads, resulting from the calculations made considering the assumptions above. It can be noted that the refrigeration thermal power of the chiller is equal to 1.92 kW, with a maximum value of the absorbed electrical power of 0.79 kW, which is equal to approximately half of the maximum value of the power absorbed by the chiller in the case without cold storage. Furthermore, it is possible to note the peak-shaving effect due to the presence of the cold storage. Fig. 10 shows, for each hour of the day, the resulting minutes of chiller operation. It can be noted that, with the adopted operational approach, the chiller operation is continuous and without stops for most of the day, and that the chiller production remains concentrated in the peak hours. Fig. 11 shows, for each hour of the day, the difference between the chiller cold generation and the cooling load. The total amount of cold to be accumulated is equal to 6.3 kWh, which represents about 18 % of the daily refrigeration thermal load of the user.

Considering the above assumptions and findings, the design value of the power supplied by the chiller, and of the volume of PCM in the 320-liter water tank, shown in Fig. 5, were calculated through the following two steps: simulation of the operation of the chiller and of a hypothetical cold storage tank having only water as storage material; calculation of the number of aluminum bottles of PCM to be inserted inside the tank considering the actual dimensions of the tank (320*l*). The results indicate that, in the case with cold storage, it is necessary to have a chiller, equipped with an inverter, characterized by a maximum absorbed electrical power of approximately 0.96 kW, which is still much lower than that of the case without storage, i.e. 1.60 kW. As to the cold storage, the resulting volume of PCM in the 320 l tank is equal to 114 l of liquid PCM, namely 120 1-litre aluminum bottles filled at 95 %, in order to

Fig. 5. Photo of the tank.

avoid the bottle rupture due to pressure variations during solidifications/melting, and 193 l of water.

Figs. 12 and 13 show the experimental results obtained using 55 PCM bottles instead of 120, used for the experimental validation of the simulation model reported in the following sections. Many consecutive standard days were simulated to establish chiller operation periodicity, ad all results reflect periodic chiller operation starting from the second day. The chiller operates continuously, with the entire water flow rate directed first to the heat exchanger simulating the cooling load and then to the cold storage tank, at 7 °C and 0.075 kg/s. Fig. 12 displays the hourly averages of cooling thermal energy in the tank, while Fig. 13 shows hourly averages of chiller-generated cooling power.

Fig. 14 shows a simplified sketch relative to the operation during the experimental test. During off-peak hours, in which the user cooling load is relatively low, the temperature at the user exit is low enough to permit the charging of the cold storage. Conversely, during on-peak hours, the temperature at the user exit is relatively high, and the cold storage is discharged. In practice, adopting this operational approach, the proper sizing of the cold storage, both in terms of PCM choice and tank sizing, would drastically reduce temperature and temperature fluctuation at the chiller inlet.

Fig. 6. Aluminum bottle containing the PCM.

Table 1
Thermophysical properties of PCM.

Property	Value
Melting temperature (°C)	15
Latent heat (kJ kg^{-1})	182
Thermal conductivity (W m^{-1} K^{-1})	
Solid	0.25
Liquid	0.15
Density (kg m^{-3})	
Solid	950
Liquid	860
Specific heat (J kg^{-1} K^{-1})	
Solid	2250
Liquid	2560

3. Numerical testing

3.1. Modeling of the cold-water TES with PCM bottles

The modeling study involved 55 PCM bottles arranged in the tank with a stratified configuration across three distinct layers: the first layer contained 19 bottles, the second had 21 bottles, and the third layer included 15 bottles. Each bottle has dimensions of 15.6 cm in height and 8.8 cm in diameter. The thermal behavior within each tank node, which is occupied by a segment of the PCM layers, is described by the following

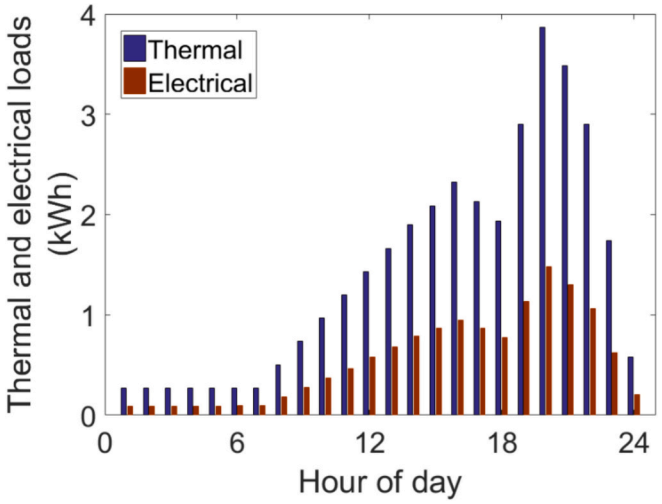

Fig. 7. Air conditioning requirements for summer cooling.

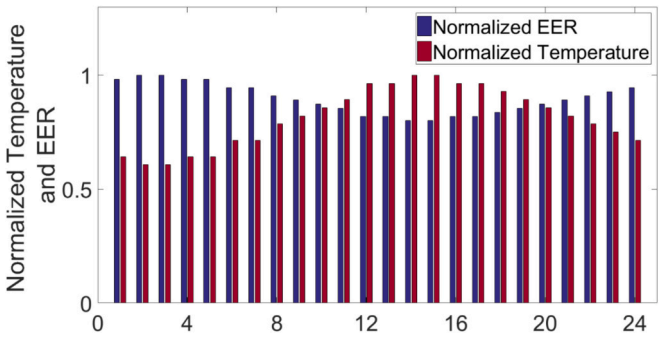

Fig. 8. Normalized EER and ambient temperature.

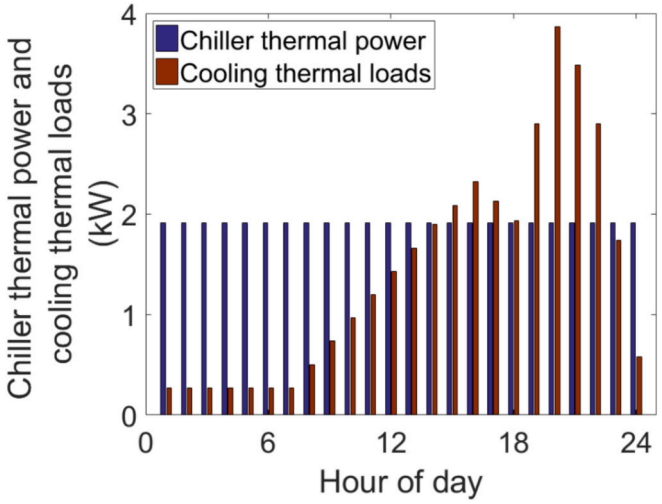

Fig. 9. Chiller cooling capacity and thermal cooling demands.

balance equation:

$$\rho_w c_w V_w \frac{dT_w}{dt} = \frac{\overline{T}_{PCM} - T_w}{R_{PCM}} + \dot{Q}_{cond} - \frac{T_w - T_{amb}}{R_{tank}} \quad (1)$$

In this equation, ρ_w and c_w represent the density and specific heat of water, respectively. V_w denotes the water volume, T_w is the water temperature, Q is the heat conducted to the adjacent node, T_{amb} is the ambient temperature, and R_{tank} is the total thermal resistance of the tank walls. For each node in the tank, the parameter T_{PCM} corresponds to the average surface temperature of the PCM bottles within that specific layer of the node. This temperature was determined through simulations using COMSOL software. The parameter R_{PCM} indicates the thermal resistance of the PCM layer present in the tank node and was calculated

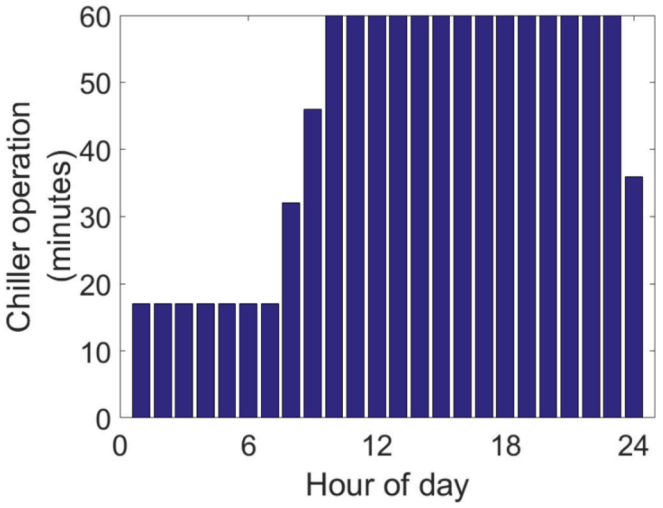

Fig. 10. Duration of chiller operation.

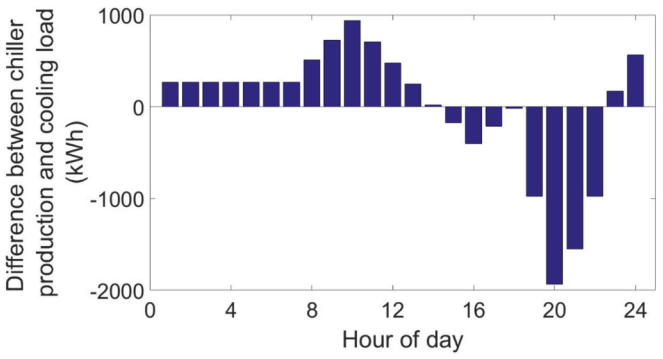

Fig. 11. Difference between cooling energy generation and thermal cooling demands.

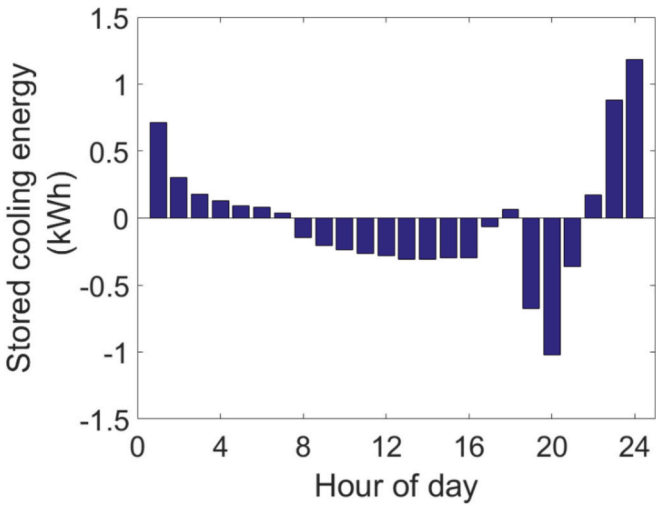

Fig. 12. Hourly averages of the refrigerant thermal energy stored.

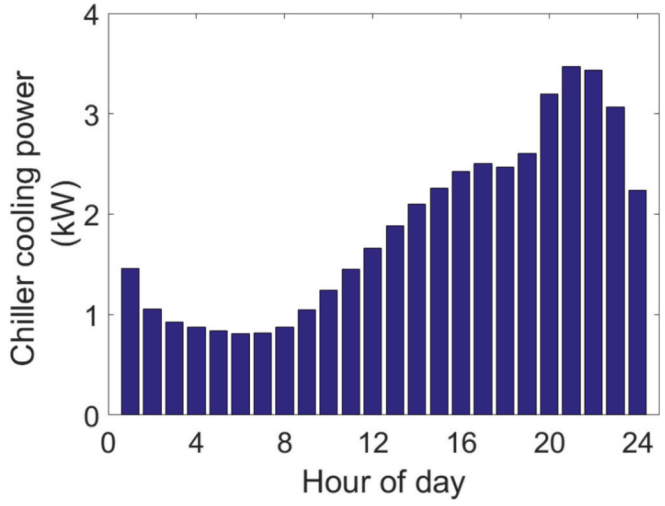

Fig. 13. Average cooling thermal power produced by the chiller on an hourly basis.

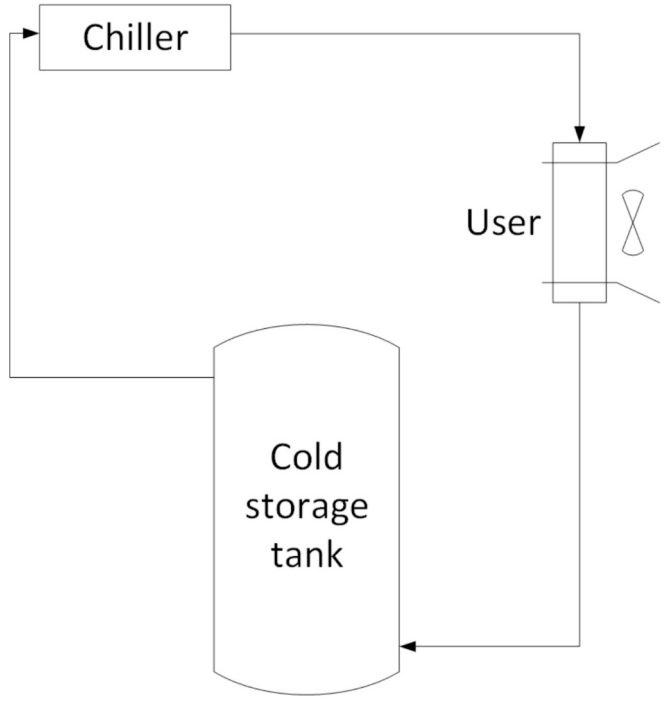

Fig. 14. Simplified sketch of the system operation during the experimental test.

using an iterative code that considers natural convection effects. Eq. (1) was solved using the Euler method for each time step and node. To accurately represent the influence of natural convection, the reversion-elimination algorithm was employed. This approach allows for the consideration of temperature variations and convective effects occurring between different layers of water at varying heights within the tank.

3.2. Model for the PCM bottles

The modeling of the cylindrical PCM module was conducted using a 2D axisymmetric computational domain, based on several key assumptions:

- homogeneous isotropic material
- uniform initial temperature
- negligible convective motions
- fixed temperature range for phase transition.

The following fundamental equations were employed in the modeling process [34]:

- energy equation

$$\rho_{PCM} c_{p,PCM,e}\left(\frac{\partial T}{\partial t}+\bar{v}\cdot\nabla T\right)=\nabla\cdot(k_{PCM}\nabla T) \tag{2}$$

- continuity equation

$$\nabla\cdot\bar{v}=0 \tag{3}$$

- momentum equation

$$\rho_{PCM}\left(\frac{\partial\bar{v}}{\partial t}+\bar{v}\nabla\cdot\bar{v}\right)=-\nabla p+\mu_{PCM,e}\nabla^2\bar{v}+\overline{F_b} \tag{4}$$

In which, p is the pressure, $\mu_{PCM,e}$ is the effective dynamic viscosity of the PCM, and $\bar{v}$ represents the velocity vector. The momentum equation, Eq. (4), incorporates the Boussinesq approximation to account for buoyancy effects caused by temperature-induced density variations. This approximation is represented by the term:

$$\overline{F_b}=\rho_{PCM}\bar{g}\beta(T-T_M) \tag{5}$$

where g is the acceleration due to gravity and β is the coefficient of thermal expansion. As a consequence of Boussinesq approximation, the PCM density is assumed to be constant throughout the computational domain and equal to the mean value between the liquid and the solid ones. Further, the volume of the computational domain was calculated and fixed in order to maintain the same mass of PCM. To accurately model the phase change behavior, the effective heat capacity method was employed. In the model equations, a smooth version of the Heaviside function with a continuous second derivative is adopted in order to analytically represent the melt fraction dependence on the temperature in the mushy zone:

$$\varphi(T)=H(T-T_M) \tag{6}$$

To simulate the phase change process, the effective heat capacity method (EHC) is implemented, according to which the material effective heat capacity ($c_{p,PCM,e}$) depends on the material heat capacity ($c_{p,PCM}$) and on the latent heat of fusion (L_h) of the PCM, as follows:

$$c_{p,PCM,e}=c_{p,PCM}+L_h\frac{d\varphi(T)}{dT} \tag{7}$$

The effective viscosity of the PCM was determined according to Eq. (8) and the parameter S was calculated using Eq. (9) to impose a zero velocity in the solid region of the PCM.

$$\mu_{PCM}=\mu_L(1+S(T)) \tag{8}$$

$$S(T)=C\frac{(1-\varphi(T))^2}{\varphi(T)^3+\delta} \tag{9}$$

In Eq. (9), C and δ are arbitrary constants: δ is typically set to 10^{-3}, while C adjusts the velocity variation in the phase transition zone and was set to $10^{3.6}$ for the charging phase and to $10^{4.2}$ for the discharging one [35]. As assessed in many works, among which the review of Hu e al. [36], and the work of Pan et al. [37], this approach would also account for the solid sinking in CCM (Close-Contact Melting).

3.2.1. Numerical implementation

The governing equations are solved using the finite element solver available in COMSOL Multiphysics 6.2. To handle the non-linearity of the equation system, a segregated approach is employed. Time

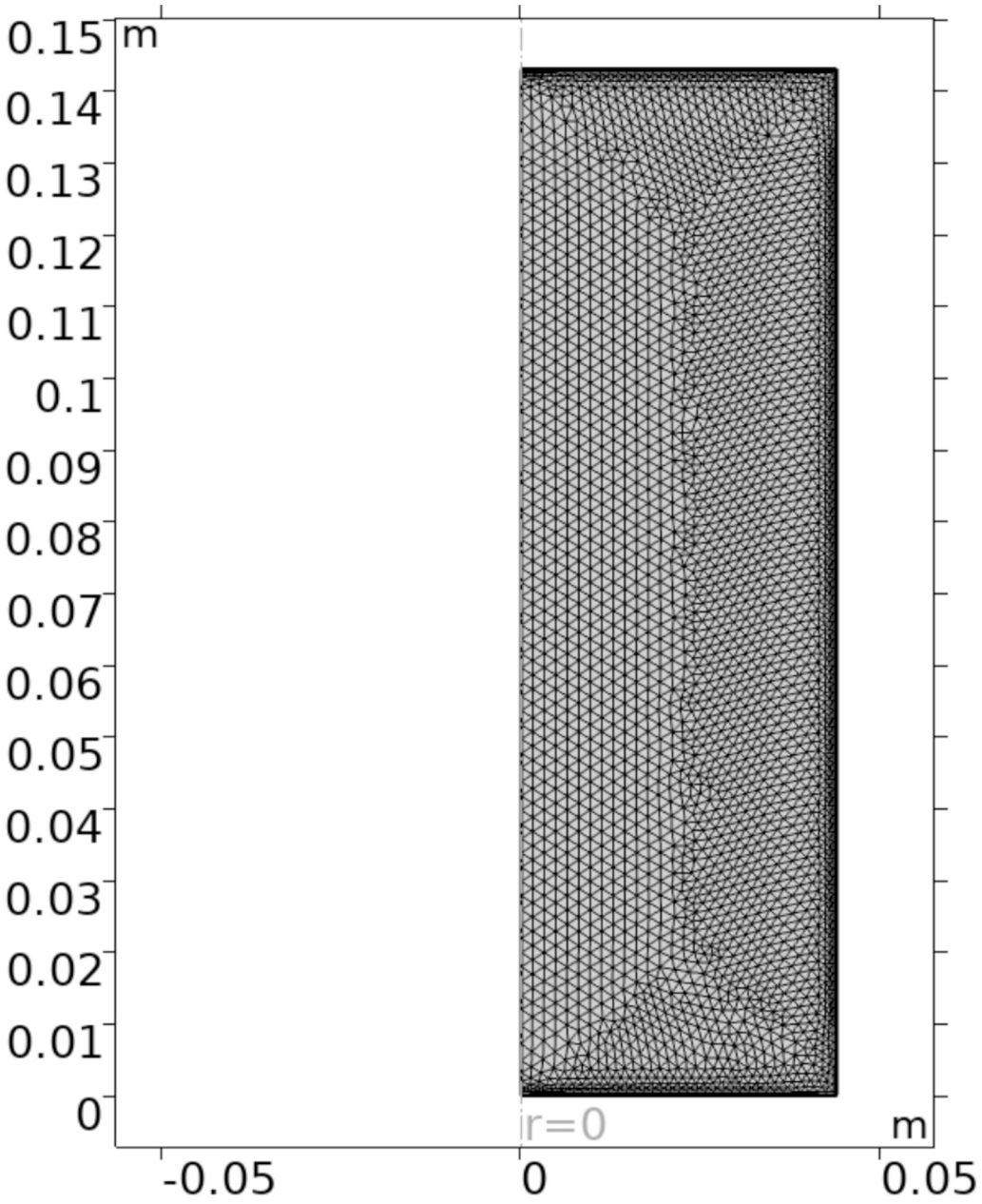

Fig. 15. Meshed computational domain.

integration is carried out using the backward differentiation formula (BDF), with an initial time step set to 10^{-4} s and no-fixed maximum time step. Physics-controlled triangular meshes are applied, and numerical experiments have been conducted to verify that the simulation results are mesh independent. Fig. 15 shows the 2D axisymmetric meshed computational domain used for the numerical simulation, consisting of 6037 domain elements and 267 boundary elements. All simulations are executed on a Dell Precision T7610 workstation, which features two Intel Xeon E5-2687W v2 processors and 64 GB of RAM operating at 1866 MHz.

3.2.2. Initial and boundary conditions

The initial and boundary conditions for each PCM module were established based on experimental tests. Specifically, these conditions account for the water temperature in the tank at the initial moment and at all subsequent times. More precisely, the initial temperature of each PCM layer, $T_{in,PCM}$, was set equal to the average temperature of the water in the tank nodes occupied by that layer, $T_{m,w,l}$, as reported in Eq. (10). For the boundary conditions, thermal flux through the lower wall, $q_{wall,BOT}$, and side wall, $q_{wall,LAT}$, of the PCM modules were specified, considering the presence of natural convection, according to Eq. (11), while the upper wall of the PCM modules was treated as adiabatic.

$$T_{in,PCM} = T_{m,w,l} \tag{10}$$

$$q_{wall,LAT,BOT} h_{LAT,BOT} \left(T_{wall,LAT} - T_{PCM}\right) \tag{11}$$

The convective heat transfer coefficients relative to the lateral and bottom surfaces of the PCM, h_{LAT} and h_{BOT}, are evaluated using the correlations for natural convection provided by the COMSOL solver.

3.3. Coupling of models

The models for the water tank and the PCM module were coupled using an iterative procedure. Initially, the tank was simulated

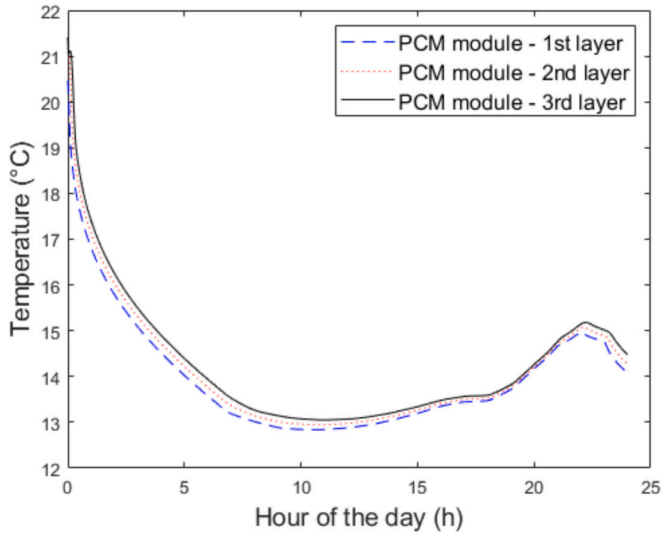

Fig. 16. Trend of the average temperature in the PCM module across all three layers of the tank over time.

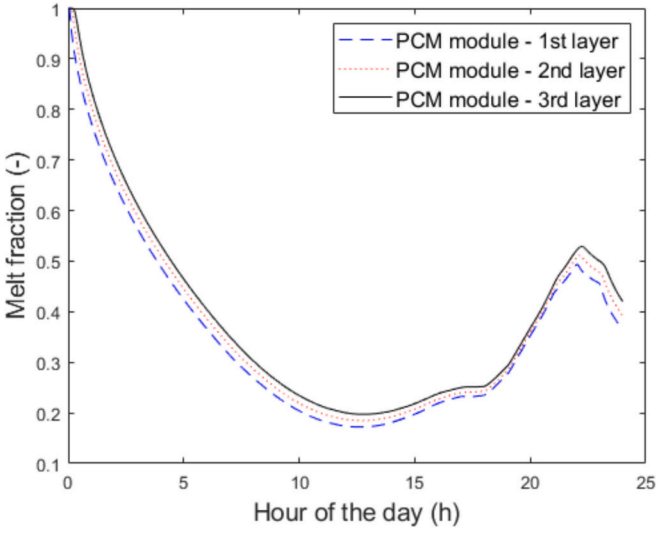

Fig. 17. Trend of the average melt fraction in the PCM module across all three layers of the tank over time.

independently, without the PCM modules. In the next step, each PCM layer was simulated with the water temperatures from the tank obtained in the previous iteration serving as boundary conditions. Following this, the water tank simulation was repeated, incorporating the average surface temperatures of the PCM modules, as determined by the COMSOL simulation. This updated simulation used the new PCM temperatures, the overall thermal transmittance between the water and the PCM, and the ambient temperature as inputs. This iterative process continued, with each PCM simulation using the latest temperature values, until convergence was achieved. The entire simulation was conducted over a 24-hour period.

4. Results and discussion

This section outlines the key findings of the analysis conducted. It begins with a presentation and discussion of the results obtained from the numerical analysis. Following this, a comparison is made between the water temperature at the tank outlet as determined by numerical simulations and the temperatures observed in experimental tests.

For the numerical modeling, key metrics are analyzed for the three PCM layers inside the tank, including average temperature, average melt fraction, and the energy stored and released by a representative PCM module for each layer. Colorimetric maps illustrate temperature distributions and melt fractions at critical moments: the start and end of the cycle, along with two other significant time points.

The experimental validation compares the outlet water temperatures from the tank obtained through numerical simulations with those measured experimentally. This comparison is based on data from tests conducted at the Thermal Energy Storage Testing Laboratory at the ENEA Research Center in Portici, where the system underwent a 13-hour charging period, a 9-hour discharging period, and an additional 2-hour charging phase. Accurate simulation was ensured by recalculating water temperature values and convective conductance for each iteration, aligning the boundary conditions with real operating conditions and allowing for a precise comparison between numerical and experimental data.

4.1. Numerical findings

4.1.1. Temperature variation

Fig. 16 illustrates the average temperature variations of the PCM module across Layers 1, 2, and 3 throughout the cycle. The figure provides a clear comparison of temperature trends among the three layers, highlighting how their positions within the tank affect their thermal behavior over time.

The data reveals that Layer 3, positioned at the top of the tank and closest to the warmer region, consistently exhibits a slightly higher average temperature compared to the other layers. This difference is particularly noticeable at both the beginning and the end of the cycle. In contrast, Layer 1, located at the bottom of the tank, generally maintains lower temperatures throughout the cycle. This is due to its reduced exposure to the heat source compared to the higher layers. Layer 2, situated midway within the tank, shows average temperatures that fall between those of Layer 1 and Layer 3. This layer responds moderately to temperature changes, reflecting its intermediate position between the warmer top layer and the cooler bottom layer. Overall, Layer 3, being in direct contact with the warmer section of the tank, exhibits the highest average temperatures. The temperature variations in this layer are most pronounced at the beginning and end of the cycle, indicating its greater sensitivity to thermal changes compared to the other layers.

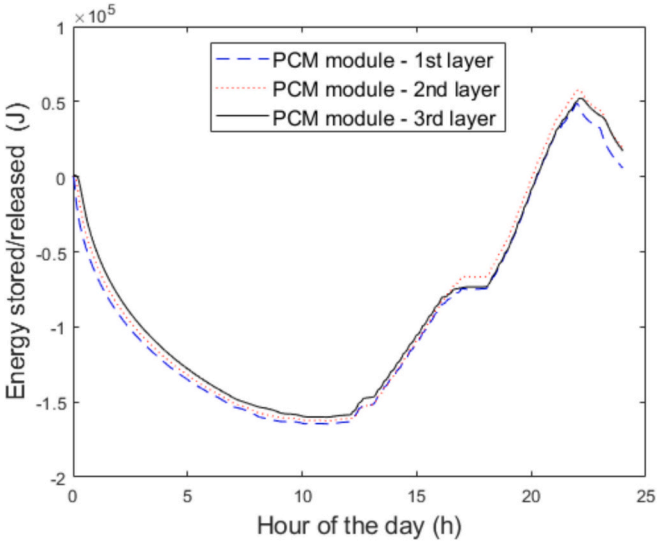

Fig. 18. Trends in the energy stored/released by the PCM module across all three layers of the tank over time.

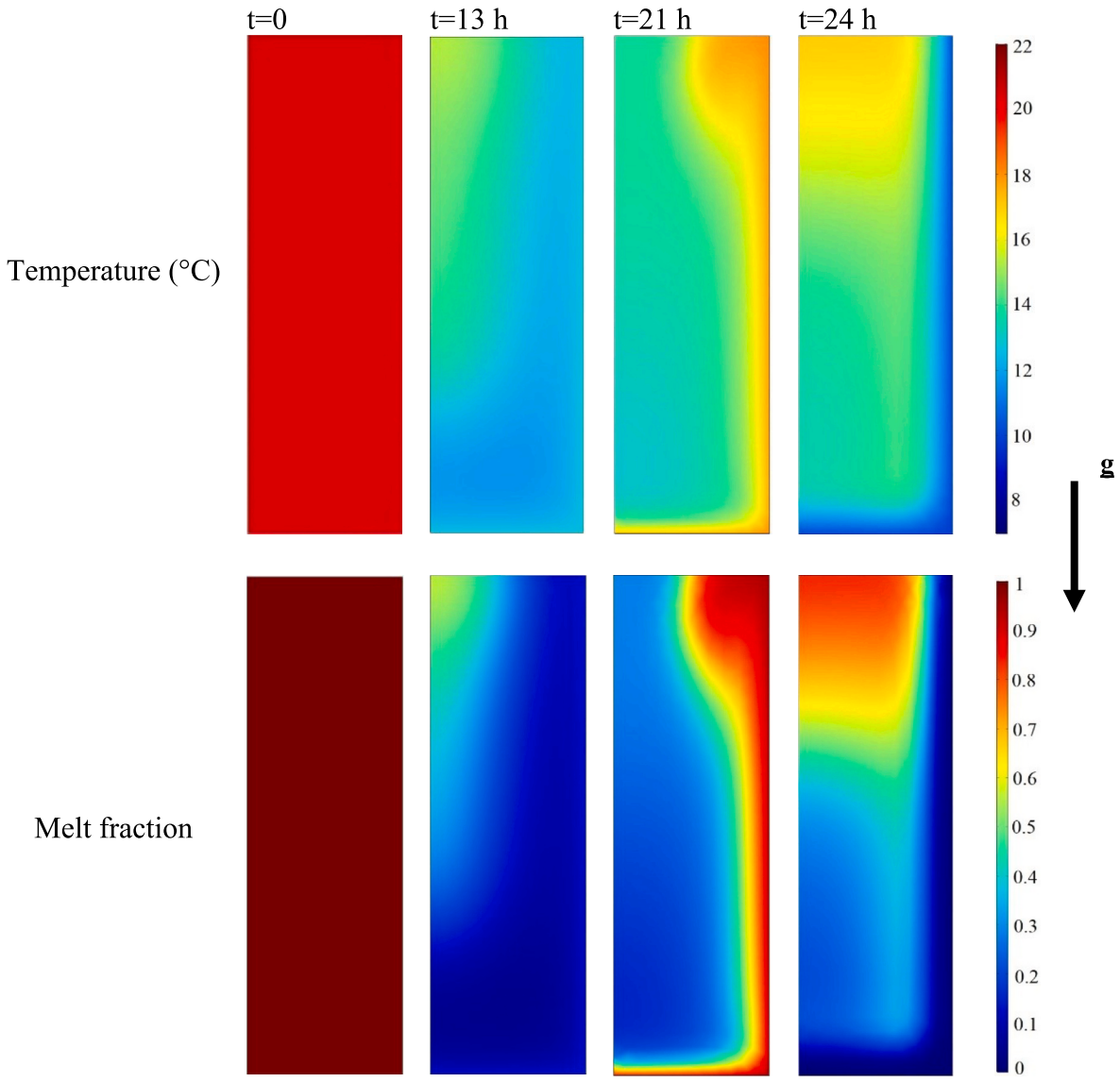

Fig. 19. Colorimetric maps of temperature and melt fraction related to a PCM module within Layer 1.

4.1.2. Melt fraction variation

Fig. 17 depicts the temporal variation in the average melt fraction within the PCM module across Layers 1, 2, and 3 throughout the cycle. It clearly demonstrates that the PCM experiences incomplete charging and discharging phases. The figure shows how temperature differences between layers significantly influence the solidification and melting phases of the PCM, with the lower-temperature first layer exhibiting a higher degree of solidification compared to the upper layers.

Specifically, the material in the modules undergoes a charging phase lasting approximately 13 h, followed by a discharging phase of about 9 h. The charging process then resumes around the 22nd hour of the day. This pattern reveals that during the charging phase, the PCM does not fully melt, and during the discharging phase, it does not completely solidify. A detailed analysis indicates that Layer 1, with its lower average temperature, shows the greatest degree of solidification. The minimum average melt fraction (ϕ average) for Layer 1 is 0.175. For Layer 2, the minimum value is slightly higher at 0.185, while for Layer 3, with its higher average temperature, the minimum value is 0.197.

4.1.3. Variation of energy accumulated/discharged

Fig. 18 illustrates the variation in energy accumulated and released by the PCM module across Layers 1, 2, and 3 throughout the cycle. By convention, accumulated energy is shown as negative, while released energy is positive. The figure demonstrates how energy is managed across the different layers of the PCM module. It is evident from the figure that there are no significant differences in energy accumulation and release among the three layers. The energy stored is about -1.5×10^5 J, while the released one is about 0.5×10^5 J. This suggests that the PCM module exhibits relatively uniform thermal behavior across the layers, indicating consistent energy management throughout the cycle.

4.1.4. Colorimetric maps

Figs. 19, 20 and 21 show the colorimetric maps for temperature and melt fraction for a PCM module for Layer 1, 2 and 3, respectively, evaluated at four significant time points: initial ($t = 0$ s), final ($t = 24$ h), and two intermediate points corresponding to the peak charging ($t = 13$ h) and peak discharging ($t = 21$ h) of the module. These time points are essential for understanding the thermal and phase behavior of the PCM within each layer.

All three layers start with high temperatures, experience cooling around 13 h, peak in warmth at 21 h, and return to lower temperatures by 24 h. Layers 2 and 3 show more localized heating/cooling, while Layer 1 displays broader shifts. Similarly, all layers show similar phase change behavior: starting as mostly solid, moving toward a balanced

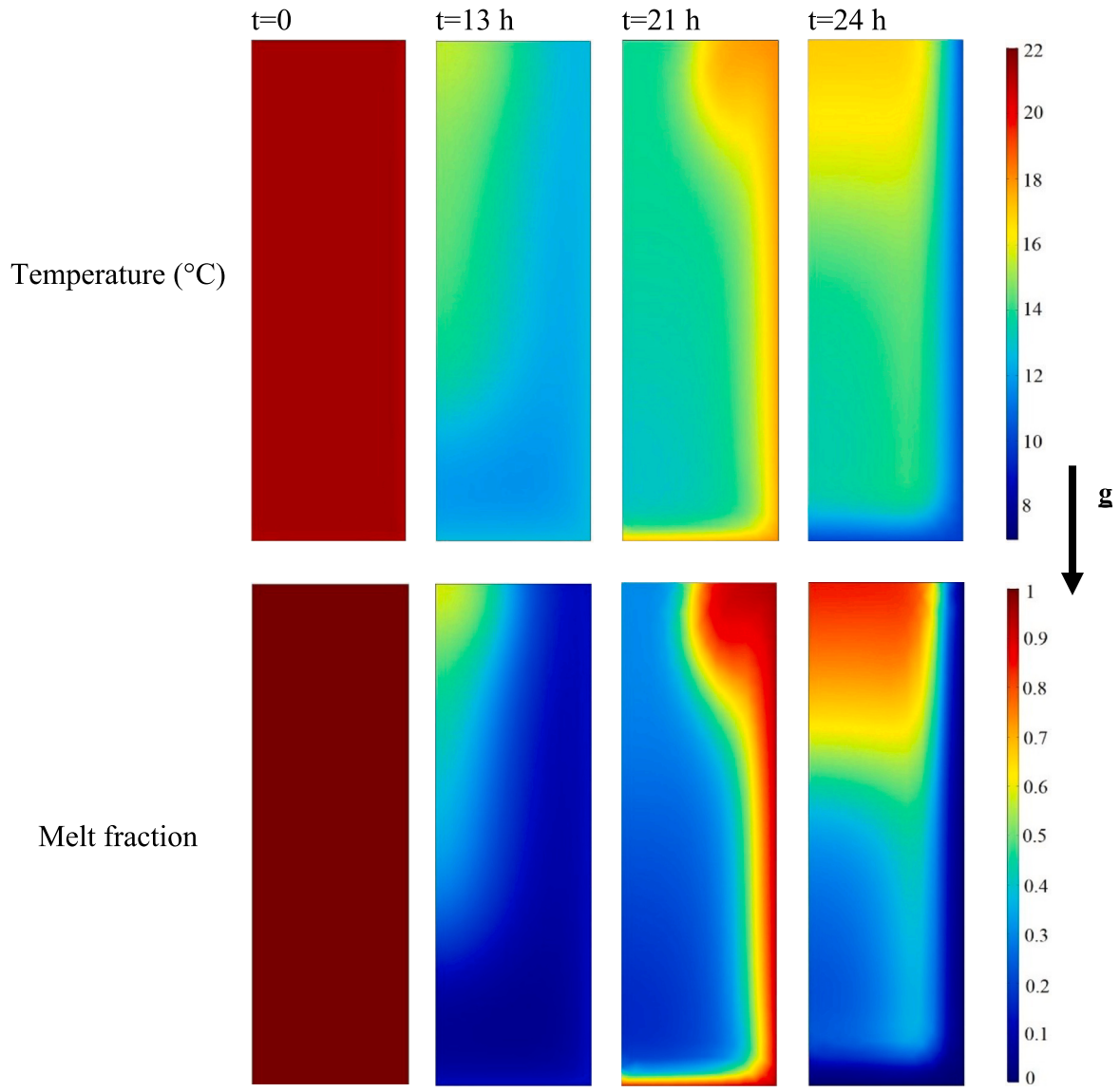

Fig. 20. Colorimetric maps of temperature and melt fraction related to a PCM module within Layer 2.

melt around 21 h, and partially solidifying again by 24 h. However, Layer 2 tends to have a slightly higher melt fraction during peak periods than the others. Tables 2 and 3 report a structured summary and comparative analysis across Layer 1, Layer 2, and Layer 3 regarding temperature variation and melt fraction variation over time, respectively.

The analysis of the colorimetric maps reveals that the differences in PCM behavior among the three layers are most pronounced in Layer 1. Specifically, Layer 1 exhibits a greater fraction of solid PCM compared to the other layers. Despite variations in temperature and melt fraction, none of the layers fully solidifies or melts during the observed period. These findings are crucial for optimizing the application of PCM modules in systems requiring precise thermal management.

4.2. Comparison between numerical and experimental data

The validation of the model was conducted by comparing the outlet water temperatures from the tank, as predicted by numerical simulations, with experimental data collected during tests. The results of this comparison are illustrated in Fig. 20a) and b).

Fig. 22a) shows a detailed comparison between the experimental data and the numerical simulations over the entire test cycle. The visual comparison reveals a good agreement between the two datasets, indicating that the numerical model accurately reflects the real-world conditions observed in the experiments. This close match underscores the precision of the thermal behavior simulation. Fig. 22b) depicts the trend of the average relative error between the numerical and experimental results. The average relative error is calculated to be 0.032, signifying a minimal discrepancy between the simulated and actual data. This low error value affirms the reliability of the numerical model and its capability to provide an accurate representation of the observed phenomenon.

5. Parametric analysis

The parametric analysis aimed to evaluate the energy performance of a cold storage system by varying the size and number of PCM bottles. The objective was to identify the best configuration - both in terms of the size and number of PCM bottles - to maximize thermal exchange efficiency for the specific case study. To achieve this, the application previously developed was updated to accommodate various storage system configurations.

The scenarios analyzed were based on a base scenario experimentally studied at the ENEA Portici Research Center. Building on this, four

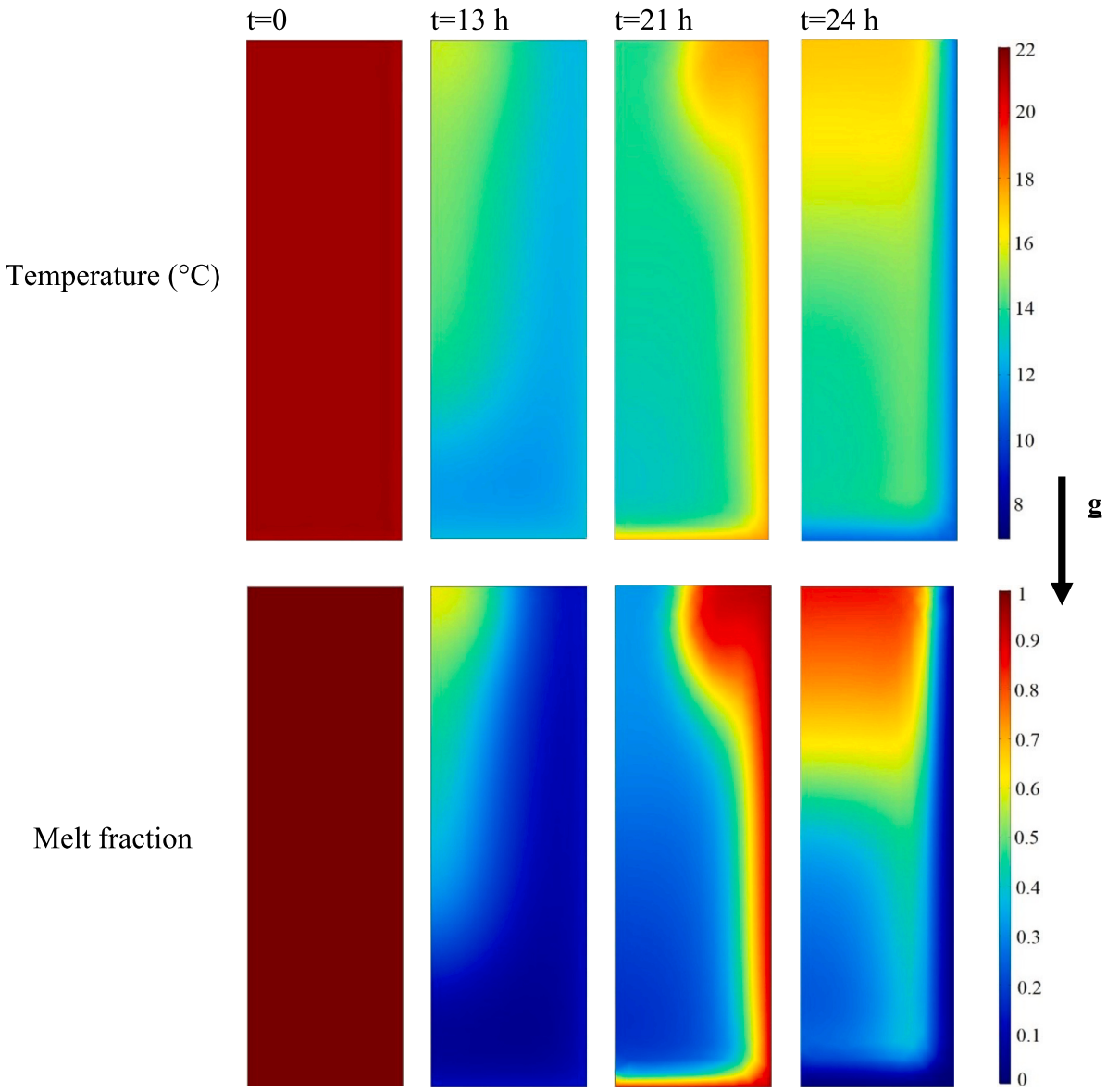

Fig. 21. Colorimetric maps of temperature and melt fraction related to a PCM module within Layer 3.

additional scenarios were examined, labeled as scenario 1, scenario 2, scenario 3, and scenario 4. The dimensions used in the analysis corresponded to commercial container sizes.

In all scenarios, the simulation duration was set to 48 h with a results visualization time step of 100 s. For the scenario used for experimental comparison, the simulation duration was extended to 72 h.

5.1. Base scenario – 1 L bottles

The scenario experimentally analyzed featured a 423-liter stainless steel water tank containing 119 aluminum bottles, each with a capacity of 1 l, a height of 20.0 cm, and an internal diameter of 8.8 cm. Each bottle was partially filled with 817 g of PCM. Thus, the height of the PCM inside each bottle was calculated and equal to 14.3 cm. The model was configured to reflect the actual positioning of the bottles inside the tank, which was divided into 6 water layers, each occupied as follows:

Starting from the bottom of the tank (total of 54 bottles):

- 25 bottles in the 1st layer
- 19 bottles in the 2nd layer
- 10 bottles in the 3rd layer.

Starting from the top of the tank (total of 65 bottles):

- 25 bottles in the 1st layer
- 25 bottles in the 2nd layer
- 15 bottles in the 3rd layer.

Also in this case, in the experimental test, the chiller operates continuously, with the entire water flow rate directed first to the heat exchanger simulating the cooling load and then to the cold storage tank, at 7 °C and 0.075 kg/s.

Fig. 23 shows a comparison between the temperature profile of the water exiting the tank from the numerical simulations and the experimental data. The figure shows an excellent match between the numerical results and the experimental measurements, with a maximum deviation of less than 1 °C observed at the temperature peaks. This confirms the accuracy of the model in representing the baseline case.

5.2. Additional scenarios

5.2.1. Scenario 1 – ½ L bottles

In the case of using bottles with a volume of ½ liter, it was assumed

Table 2
Temperature variation summary for the three layers.

Time (h)	Layer 1	Layer 2	Layer 3
0	Uniform temperature distribution across the PCM module, with areas in red indicating the highest temperatures.	Similar to Layer 1.	Similar to Layer 1.
13	Broader areas of blue and green, which indicate lower temperatures compared to the initial state.	Increased areas of blue and turquoise indicating lower temperatures.	Increase in lower temperature areas, with a predominance of green and turquoise.
21	More pronounced variation, with a predominance of yellow areas, suggesting increased temperatures in some regions of the module.	Warming in central areas, with predominant yellow and orange tones indicating higher temperatures.	Higher temperatures in some regions, with yellow and orange tones prevalent.
24	Temperature distribution has cooled, with a predominance of green and blue tones indicating a return to lower temperatures.	More uniform temperature distribution, with predominance of green and blue, suggesting cooling.	Decrease in temperature, with green and blue tones indicating cooling.

Table 3
Melt fraction variation summary for the three layers.

Time (h)	Layer 1	Layer 2	Layer 3
0	The solid fraction is dominant, as indicated by the dark red areas on the map.	Similar to Layer 1.	Similar to Layer 1.
13	The solid fraction remains predominant, though some areas in the liquid phase (indicated by blue electric) become visible.	Increased liquid fraction, with more prominent blue electric areas showing melting.	Increased liquid fraction, with more noticeable blue electric areas showing melting.
21	More balanced distribution between solid and liquid phases, with rainbow colours indicating a mix of both.	Larger liquid fraction with rainbow areas indicating a mix of solid and liquid phases.	Balanced solid and liquid fraction, with rainbow colours indicating a mixture of both phases.
24	Increased solid fraction, with blue electric areas indicating partial solidification of the PCM.	The solid fraction is again predominant, with blue and blue electric areas indicating partial solidification.	Predominance of the solid phase, with blue and blue electric areas indicating solidification.

that the tank contained 238 aluminum bottles, each with a height of 20.0 cm and an internal diameter of 6.5 cm. Each bottle was partially filled with 408 g of PCM, ensuring that the total amount of PCM introduced into the tank was the same as in the baseline case. The PCM level in each bottle was calculated to be 13.6 cm. The tank was then divided into 6 water layers, with each layer consisting of:

Starting from the bottom of the tank (total of 108 bottles):

- 50 bottles in the 1st layer
- 38 bottles in the 2nd layer
- 20 bottles in the 3rd layer

Starting from the top of the tank (total of 130 bottles):

- 50 bottles in the 1st layer
- 50 bottles in the 2nd layer
- 30 bottles in the 3rd layer

5.2.2. Scenario 2 – ¼ L bottles

In the scenario using ¼-liter bottles, it was assumed that the tank held 476 aluminum bottles, each with a height of 17.0 cm and an internal diameter of 5.2 cm. Each bottle was partially filled with 204 g of PCM to ensure that the total amount of PCM in the tank matched that of the base scenario, resulting in a PCM height of 10.6 cm per bottle. The tank was divided into 7 layers of water as follows:

From the bottom of the tank (total of 216 bottles):

- 100 bottles in the 1st layer
- 76 bottles in the 2nd layer
- 40 bottles in the 3rd layer
- No bottles in the 4th layer.

From the top of the tank (total of 260 bottles):

- 100 bottles in the 1st layer
- 100 bottles in the 2nd layer
- 60 bottles in the 3rd layer.

5.2.3. Scenario 3–1/10 L bottles

For the scenario with 1/10-liter bottles, it was assumed that the tank contained 1190 aluminum bottles, each with a height of 10.1 cm and an internal diameter of 4.4 cm. Each bottle was partially filled with 82 g of PCM to ensure that the total amount of PCM in the tank was consistent with the base scenario, resulting in a PCM height of 6.6 cm per bottle. The tank was divided into 12 layers as follows:

From the bottom of the tank (total of 540 bottles):

- 150 bottles in the 1st layer
- 150 bottles in the 2nd layer
- 150 bottles in the 3rd layer
- 90 bottles in the 4th layer
- No bottles in the 5th, 6th, and 7th layers.

From the top of the tank (total of 650 bottles):

- 150 bottles in the 1st layer
- 150 bottles in the 2nd layer
- 150 bottles in the 3rd layer
- 150 bottles in the 4th layer
- 50 bottles in the 5th layer.

5.2.4. Scenario 4–1/636.6 L bottles

In the case with 1/636.6-liter bottles, it was assumed that the tank contained 75,803 aluminum bottles, each with a height of 2.0 cm and an internal diameter of 1.0 cm. Each bottle was partially filled with 1.28 g of PCM to ensure that the total amount of PCM in the tank was the same as in the base scenario, resulting in a PCM height of 1.8 cm per bottle. The tank was divided into 60 layers as follows:

From the bottom of the tank:

- 2900 bottles per layer from the 1st to the 12th layer
- 235 bottles in the 13th layer
- No bottles from the 14th to the 45th layer
- 168 bottles in the 46th layer
- 2900 bottles per layer from the 47th to the 60th layer.

5.3. Results

Results are presented by comparing all the analyzed cases in terms of: (i) the water temperature trend in the tank; (ii) the average

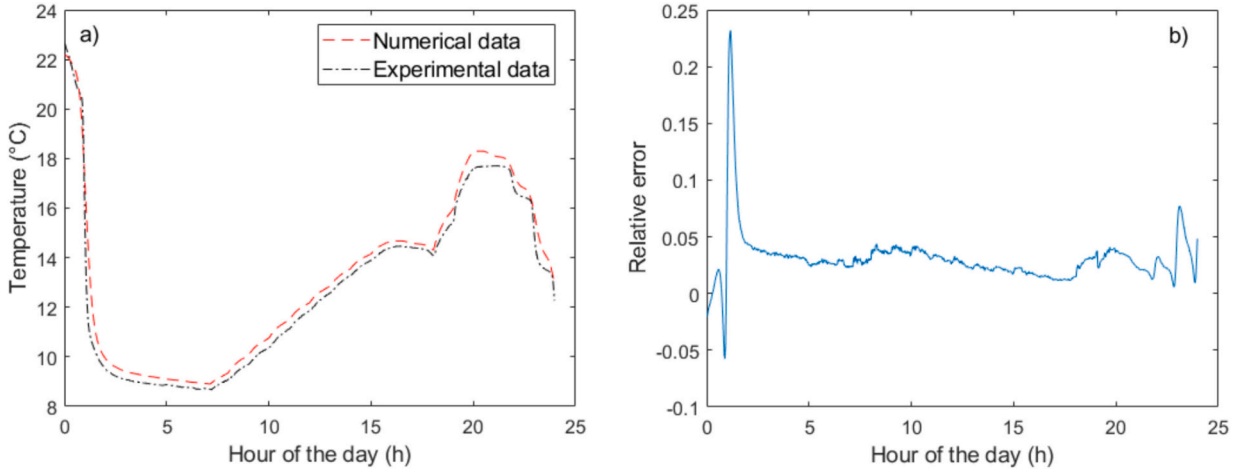

Fig. 22. a) Comparison between experimental data and numerical data. b) Average relative error.

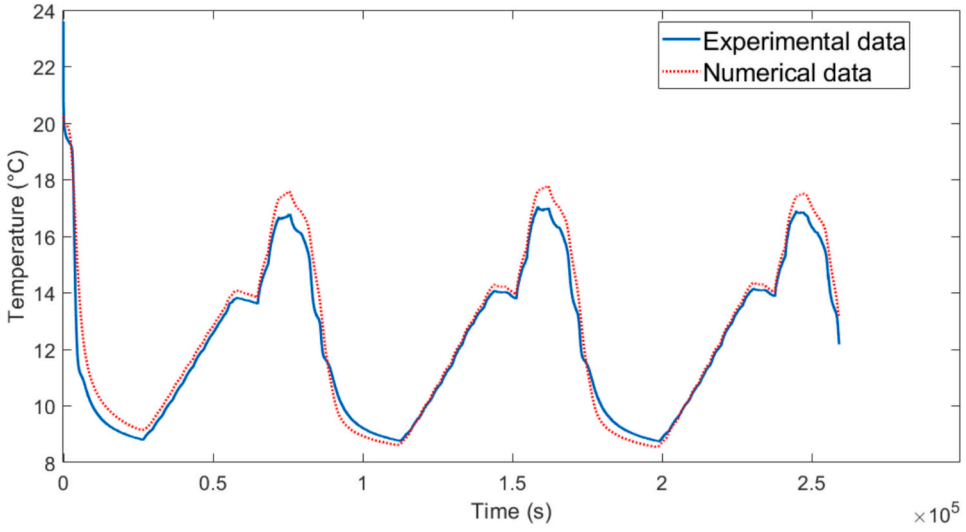

Fig. 23. Comparison of numerical and experimental results for the base scenario.

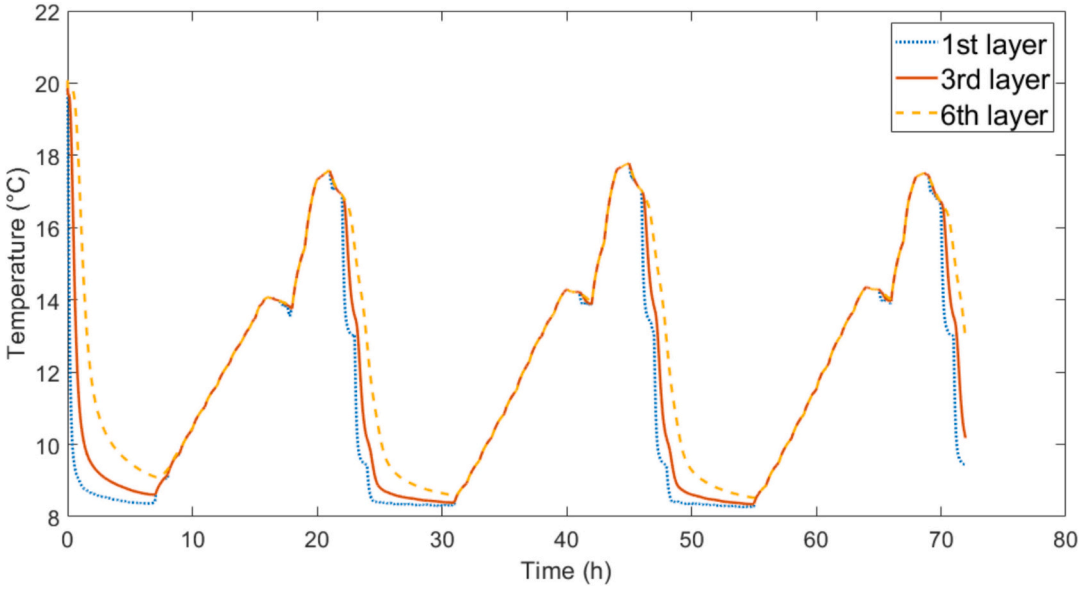

Fig. 24. Water temperature in the tank: Base scenario (1-liter bottles).

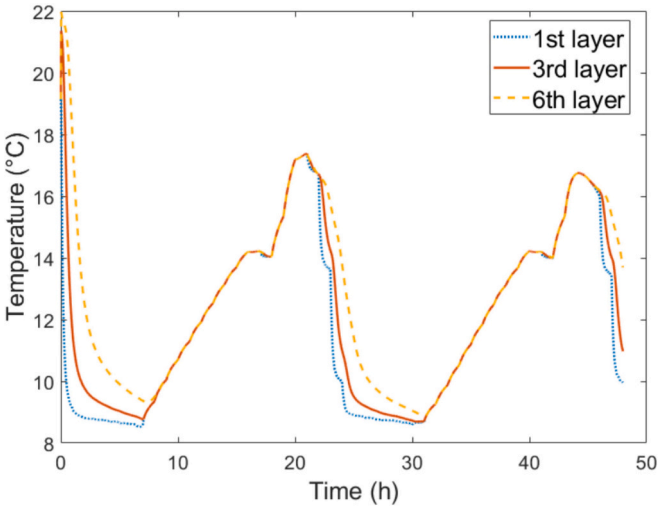

Fig. 25. Water temperature in the tank: Scenario 1 (½-liter bottles).

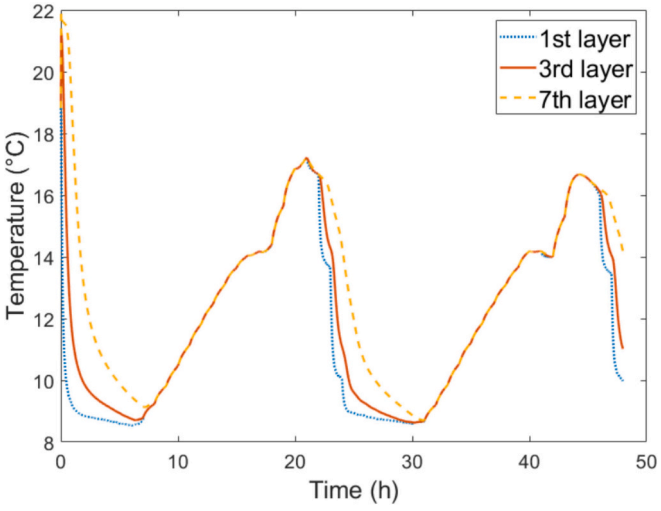

Fig. 26. Water temperature in the tank: Scenario 2 (¼-liter bottles).

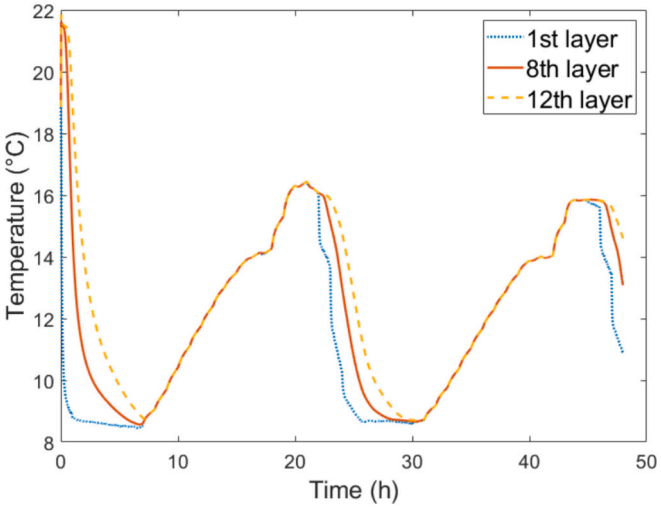

Fig. 27. Water temperature in the tank: Scenario 3 (1/10-liter bottles).

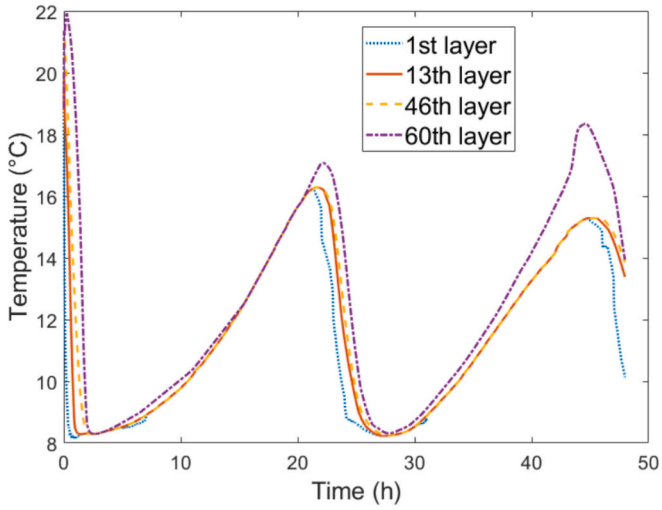

Fig. 28. Water temperature in the tank: Scenario 4 (1/636.6-liter bottles).

temperature trend in the PCM; (iii) the melt fraction trend of the PCM; (iv) the energy stored/released by the PCM module.

To simplify the discussion, these results are shown only for certain tank layers containing the PCM containers, specifically the most significant ones. For each case, the results for the 1st and last layers, as well as at least one intermediate layer, are presented. For the energy stored/released by the PCM modules, the trend is shown only for a single, centrally located layer. In the following results, the tank layers are referenced starting from the bottom. Thus, the 1st layer is positioned at the bottom surface of the tank, while the last layer is at the top.

5.3.1. *Water temperature trends in the tank*

Figs. 24–28 illustrate the temperature trends of the water inside the tank for all analyzed scenarios. As previously mentioned, only the base scenario was simulated for a period of 72 h, while the other scenarios were simulated for 48 h. These figures reveal that, despite the temperature variations being quite similar across different layers and scenarios, the upper water layers tend to have higher temperature values. This phenomenon is due to the fact that the upper parts of the tank are exposed to more heat compared to the lower parts. This behavior is particularly evident for scenario 4, where the last layer, the 60th, shows a significant increase in water temperature compared to the other layers and scenarios. Specifically, in the base scenario (Fig. 24), a gradual temperature distribution is observed, reflecting a thermal equilibrium reached over the 72 h of simulation. This scenario serves as a reference for evaluating the effectiveness and accuracy of the shorter simulations.

In scenario 1 (Fig. 25), with ½-liter bottles, the water temperature shows a trend similar to the base scenario but with slight variations due to the smaller volume. This indicates a thermal dynamic that maintains some uniformity but is affected by the change in volume. Scenario 2 (Fig. 26), with ¼-liter bottles, presents thermal trends that start to deviate more significantly from the base scenario. The reduction in volume appears to accentuate the temperature differences between the upper and lower layers. In scenario 3 (Fig. 27), with 1/10-liter bottles, there is a greater sensitivity to thermal variations, resulting in a more pronounced differentiation between the water layers. This suggests that smaller volumes can amplify heat transfer dynamics. Finally, scenario 4 (Fig. 28), with 1/636.6-liter bottles, shows a clear increase in the temperature of the last layer, the 60th. This behavior indicates a much higher thermal reactivity compared to the other cases, highlighting how a drastic reduction in volume can significantly affect the thermal dynamics of the system.

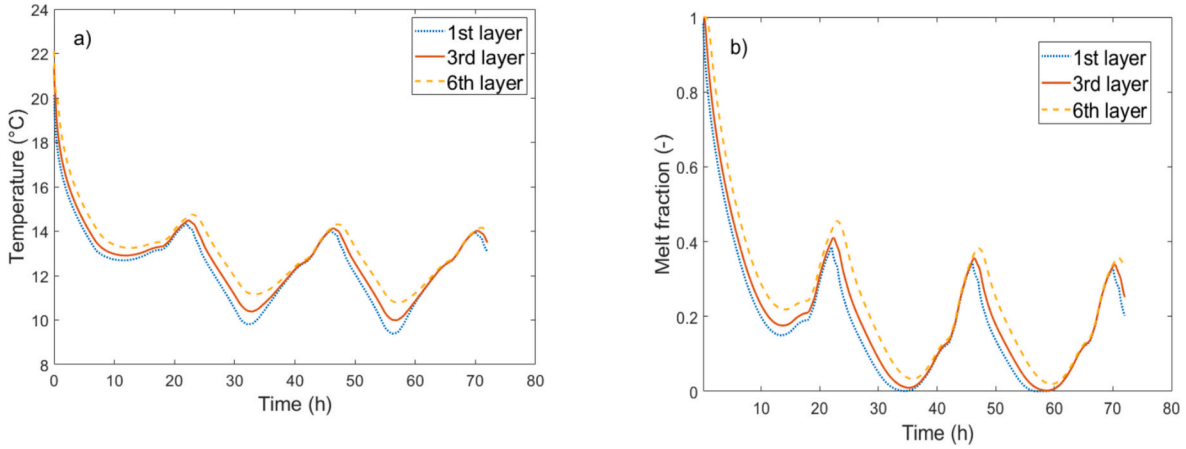

Fig. 29. a) Temperature in PCM, b) Melting fraction of PCM: base scenario (1-liter bottles).

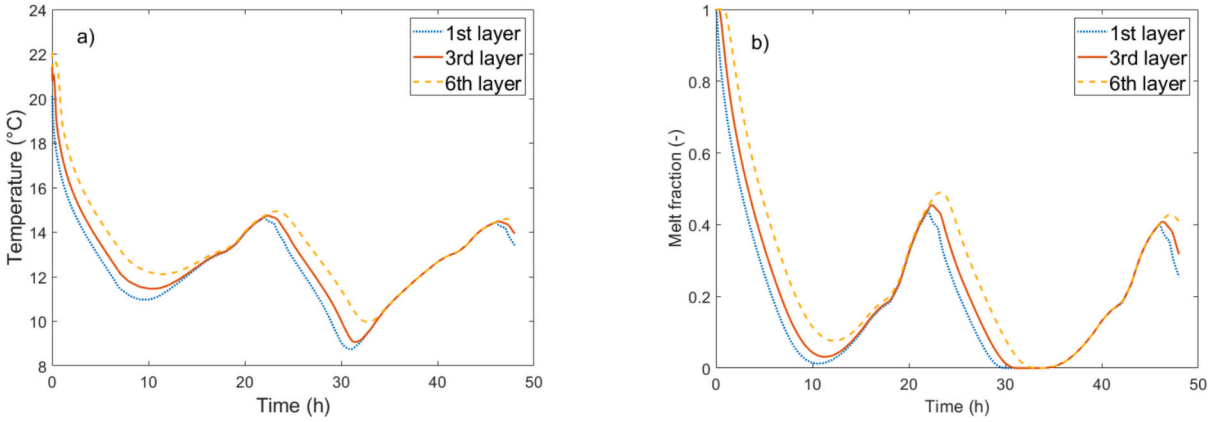

Fig. 30. a) Temperature in PCM, b) Melting fraction of PCM: scenario 1 (½-liter bottles).

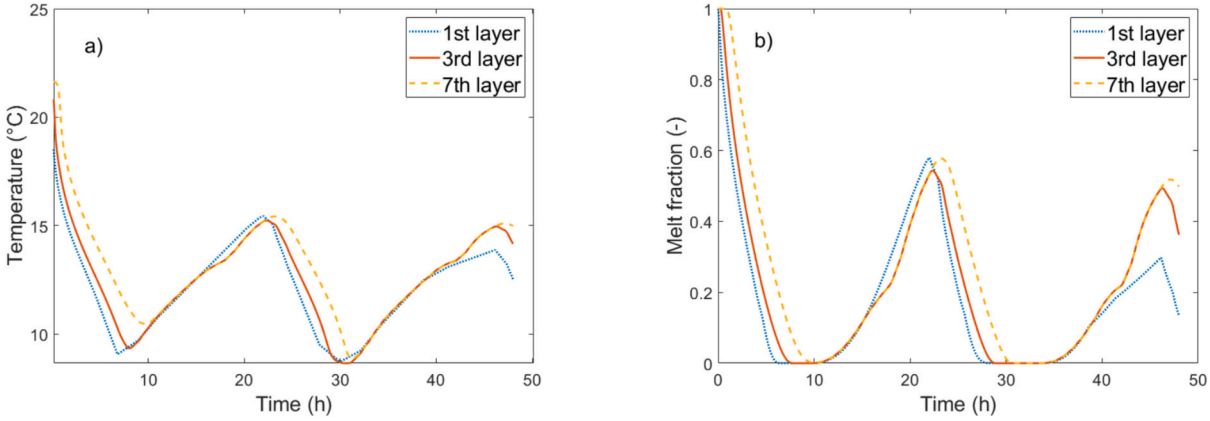

Fig. 31. a) Temperature in PCM, b) Melting fraction of PCM: scenario 2 (¼-liter bottles).

5.3.2. Trends in temperature and melting fraction of PCM

Figs. 29–33a) and b) illustrate the trends in the average temperature in the PCM module and the melt fraction of the PCM in different layers of the tank for all analyzed scenarios, respectively.

Similar to the trends observed in water temperature, the average temperatures of the various PCM layers exhibit comparable behavior. However, the figures highlight that reducing the size of the PCM bottles lowers the minimum temperature achieved. In the base scenario, the minimum temperature is around 10 °C, whereas in scenario 4, it decreases to approximately 8 °C. Furthermore, this temperature reduction occurs more rapidly with smaller bottles.

Reducing the bottle size accelerates the solidification process of the PCM. In the base scenario, the solid fraction drops to zero (or rather the PCM is completely solidified) around the 11th hour of the second day. In scenario1, this occurs around the 10th hour of the second day, with the first PCM layer reaching nearly zero by the 10th hour of the first day. In scenario 2, the solid fraction hits zero around the 9th hour of the first day; in scenario 3, around the 7th hour; and in scenario 4, around the 5th

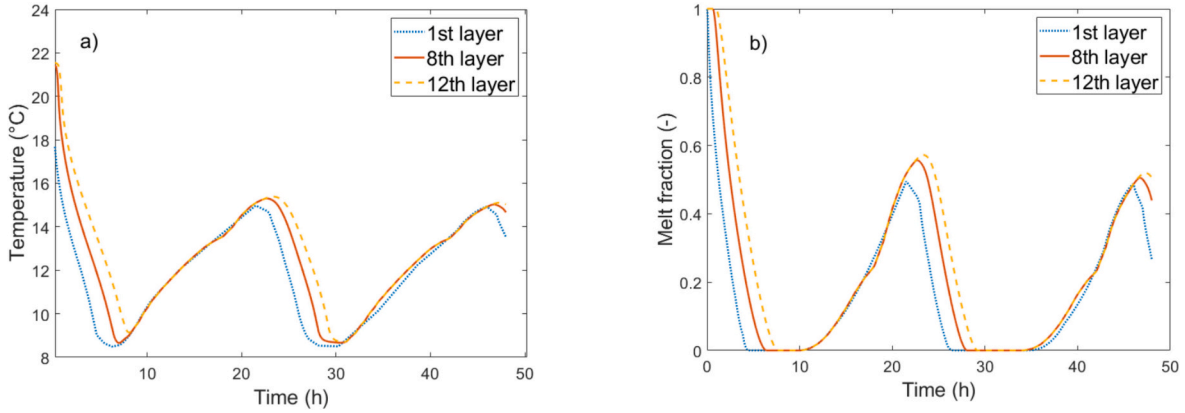

Fig. 32. a) Temperature in PCM, b) Melting fraction of PCM: scenario 3 (1/10-liter bottles).

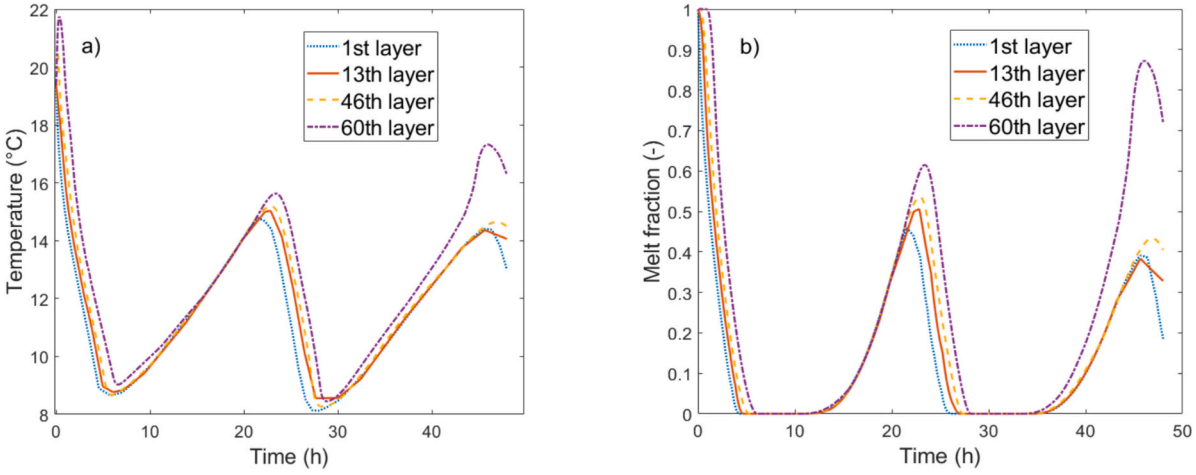

Fig. 33. a) Temperature in PCM, b) Melting fraction of PCM: scenario 4 (1/636.6-liter bottles).

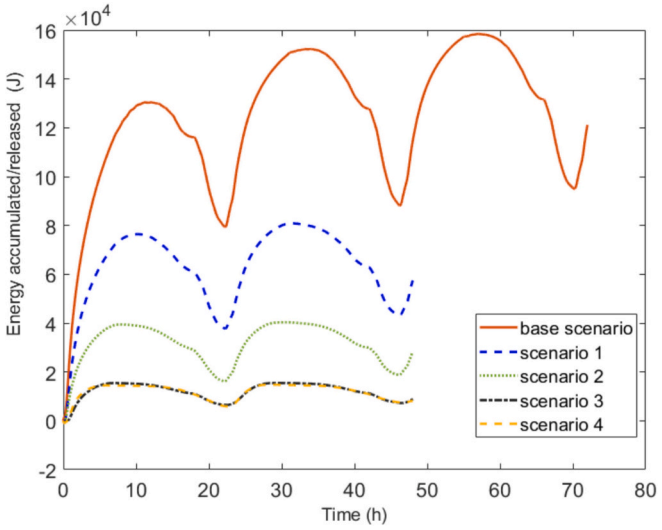

Fig. 34. Accumulated/released energy by the PCM module for all considered scenarios.

hour.

Similarly, during the discharge phase (melting of the PCM), the maximum temperature in the modules rises as the bottle size decreases. In the base scenario, the maximum temperature is approximately 14 °C, while in scenario 4, it reaches 18 °C. This increase in temperature promotes more PCM melting. The melted fraction in the top PCM layer is about 0.4 in the base scenario, 0.42 in scenario 1, 0.57 in scenario 2, 0.58 in scenario 3, and 0.87 in scenario 4.

In all analyzed cases, the upper layers of PCM in the tank exhibit higher temperatures, leading to slower solidification and faster melting. Overall, it is observed that the modules are never completely charged or discharged.

Table 4
Comparison of energy accumulation and release across the scenarios.

Scenario	Energy accumulated (kJ)		Energy released (kJ)
	Latent heat	Sensible heat	
Base	149	9	63
1	74	7	38
2	37	3	21
3	14.80	0.60	8.40
4	0.230	0.06	0.140

5.3.3. *Trends in energy accumulation and release for the PCM module*

Fig. 34 illustrates the trend of energy accumulated and released by individual PCM modules located in the central layer for all analyzed scenarios. This trend is the sum of the energy contributions recorded at each considered time interval. The figure clearly demonstrates that as the size of the modules decreases - resulting in a reduced amount of PCM in each module - both the energy accumulated, and the energy released

decrease accordingly. Table 4 summarizes the total energy accumulated and released by the modules at the beginning of the first cycle when periodic conditions are reached. The chart displays the accumulated energy (kJ) in latent and sensible forms, along with the energy released (kJ) for each scenario. The difference corresponds to the cooling energy that is lost due to initial charging. Further, as it was already clear in the previous section showing that in all cases the melted fraction doesn't reach 100 % when periodic conditions are obtained, in the analyzed configurations the full cold storage potential of PCM in terms of latent heat is not utilized. In order to fully exploit its potential, a different and optimized geometry of PCM capsules should be individuated for the present application.

6. Conclusions

This study has provided valuable insights into the performance of a Thermal Energy Storage (TES) system using water and macro-encapsulated Phase Change Materials (PCM) for cold applications. Through both experimental and numerical analyses, the research explored key aspects of the system behavior, including charging/discharging dynamics, water temperature profiles, and energy storage rates.

The primary findings are as follows:

1. **Validation of Numerical Model**: The comparison between experimental data and numerical simulations showed strong alignment, confirming the reliability of the models employed in COMSOL Multiphysics and Matlab. The low average relative error underscores the robustness of the simulation in predicting the thermal behavior of both water and PCM in the TES system.
2. **Impact of PCM Configuration**: The parametric analysis demonstrated that the size of the PCM containers significantly affects thermal performance. Smaller PCM containers, such as those with volumes of 1/10 L and 1/636.6 L, displayed faster thermal responses but lower energy storage capacity. Larger PCM containers provided slower but more stable thermal regulation, highlighting the trade-off between response speed and storage efficiency.
3. **Energy Storage and Efficiency**: None of the PCM modules achieved complete melting or solidification during the testing, suggesting that optimizing the charging/discharging cycles and PCM container sizes could enhance the system's energy storage efficiency. Larger PCM containers offered more consistent temperature regulation, while smaller ones improved heat transfer but stored less energy overall.

In conclusion, this contribution can represent a reference for the design of advanced TES systems for cold applications based on PCMs, by offering insights that can lead to the enhancement of the storage efficiency. Future research should focus on optimizing the arrangement and size of PCM bottles within storage tanks to achieve a balance between energy capacity and heat transfer, along with testing the system under varied operational conditions to refine its performance.

CRediT authorship contribution statement

M. Caliano: Writing – review & editing, Writing – original draft, Methodology, Investigation, Formal analysis, Data curation, Conceptualization. **N. Bianco:** Writing – review & editing, Validation, Supervision. **G. Graditi:** Writing – review & editing, Validation, Supervision. **L. Mongibello:** Writing – review & editing, Writing – original draft, Methodology, Data curation, Conceptualization.

Declaration of competing interest

The authors declare that they have no known competing financial interests or personal relationships that could have appeared to influence the work reported in this paper.

Acknowledgments

This research was funded by the Italian Ministry of Economic Development, within the research project “RdS-PAR 2019–2021”.

Data availability

No data was used for the research described in the article.

References

[1] M. Farid, A. Auckaili, G. Gholamibozanjani, Thermal Energy Storage With Phase Change Materials, 1st ed., CRC Press, Boca Raton, 2021.
[2] B. Zalba, J.M. Marín, L.F. Cabeza, H. Mehling, Review on thermal energy storage with phase change: materials, heat transfer analysis and applications, Appl. Therm. Eng. 23 (3) (2003) 251–283.
[3] Ibrahim Dincer, M.A. Rosen, Thermal energy storage: systems and applications, John Wiley & Sons, 2011.
[4] M.M. Farid, A.M. Khudhair, S.A.K. Razack, S. Al-Hallaj, A review on phase change energy storage: materials and applications, Energ. Conver. Manage. 45 (9–10) (2004) 1597–1615, https://doi.org/10.1016/j.enconman.2003.09.015.
[5] F.L. Rashid, A. Dulaimi, W.A. Hatem, M.A. Al-Obaidi, A. Ameen, M.A. Eleiwi, S. A. Jawad, L.F.A. Bernardo, J.W. Hu, Recent advances and developments in phase change materials in high-temperature building envelopes: a review of solutions and challenges, Buildings 14 (2024) 1582, https://doi.org/10.3390/buildings14061582.
[6] V.J. Reddy, M.F. Ghazali, S. Kumarasamy, Advancements in phase change materials for energy-efficient building construction: a comprehensive review, Journal of Energy Storage 81 (2024) 110494, https://doi.org/10.1016/j.est.2024.110494.
[7] B. Xu, P. Li, C.L. Chan, Application of phase change materials for thermal energy storage in concentrated solar thermal power plants: a review to recent developments, Appl. Energy 16 (2015) 286–307, https://doi.org/10.1016/j.apenergy.2015.09.016.
[8] M. Sheikholeslami, Application of phase change material in solar energy systems as ventilation system, in: M. Sheikholeslami (Ed.), Solar thermal systems and applications, Elsevier, 2024, pp. 235–279, https://doi.org/10.1016/B978-0-443-15838-4.00015-5.
[9] V. Bianco, M. De Rosa, K. Vafai, Phase-change materials for thermal management of electronic devices, Appl. Therm. Eng. 214 (2022) 118839, https://doi.org/10.1016/j.applthermaleng.2022.118839.
[10] C. Liu, D. Xu, J. Weng, S. Zhou, W. Li, Y. Wan, S. Jiang, D. Zhou, J. Wang, Q. Huang, Phase change materials application in battery thermal management system: a review, Materials 13 (2020) 4622, https://doi.org/10.3390/ma13204622.
[11] A. Shukla, A. Sharma, M. Shukla, C.R. Chen, Development of thermal energy storage materials for biomedical applications, J. Med. Eng. Technol. 39 (6) (2015) 363–368, https://doi.org/10.3109/03091902.2015.1054523.
[12] S.F. Li, Z. Liu, X.J. Wang, A comprehensive review on positive cold energy storage technologies and applications in air conditioning with phase change materials, Appl. Energy 255 (2019) 113667, https://doi.org/10.1016/j.apenergy.2019.113667.
[13] A.H.N. Al-mudhafar, M.T. Hamzah, A.L. Tarish, Potential of integrating PCMs in residential building envelope to reduce cooling energy consumption, Case studies in thermal engineering. Thermal Science and Engineering Progress 27 (2021) 101360, https://doi.org/10.1016/j.csite.2021.101360.
[14] H. Selvnes, Y. Allouche, R.I. Manescu, A. Hafner, Review on cold thermal energy storage applied to refrigeration systems using phase change materials, Thermal Science and Engineering Progress 22 (2021) 100807, https://doi.org/10.1016/j.tsep.2020.100807.
[15] M. Ismail, W.K. Zahra, S. Ookawara, H. Hassan, Boosting the air conditioning unit performance using phase change material: impact of system configuration, J. Energy Storage 56 (A) (2022) 105864, https://doi.org/10.1016/j.est.2022.105864.
[16] R.K. Sharma, A. Kumar, D. Rakshit, A phase change material (PCM) based novel retrofitting approach in the air conditioning system to reduce building energy demand, Appl. Therm. Eng. 238 (2024) 121872, https://doi.org/10.1016/j.applthermaleng.2023.121872.
[17] P. Charvát, L. Klimeš, M. Ostry, Numerical and experimental investigation of a PCM-based thermal storage unit for solar air systems, Energ. Buildings 68 (2014) 488–497, https://doi.org/10.1016/j.enbuild.2013.10.011.
[18] A. Allouhi, A. Ait Msaad, M. Benzakour Amine, R. Saidur, M. Mahdaoui, T. Kousksou, A.K. Pandey, A. Jamil, N. Moujibi, A. Benbassou, Optimization of melting and solidification processes of PCM: application to integrated collector storage solar water heater, Sol. Energy 171 (2018) 562–570, https://doi.org/10.1016/j.solener.2018.06.096.
[19] J. Zhao, Y. Ji, Y. Yuan, Z. Zhang, J. Lu, Seven operation modes and simulation models of solar heating system with PCM storage tank, Energies 10 (12) (2017) 21–28, https://doi.org/10.3390/en10122128.
[20] G. Bejarano, J.J. Suffo, M. Vargas, M.G. Ortega, Novel scheme for a PCM-based cold energy storage system. Design, modelling, and simulation, Appl. Therm. Eng. 132 (2018) 256–274, https://doi.org/10.48550/arXiv.2402.03395.

[21] X. Cheng, X. Zhai, Thermal performance analysis and optimization of a cascaded packed bed cool thermal energy storage unit using multiple phase change materials, Appl. Energy 215 (2018) 566–576, https://doi.org/10.1016/j.apenergy.2018.02.053.
[22] A. Raul, M. Jain, S. Gaikwad, S.K. Saha, Modelling and experimental study of latent heat thermal energy storage with encapsulated PCMs for solar thermal applications, Appl. Therm. Eng. 143 (2018) 415–428, https://doi.org/10.1016/j.applthermaleng.2018.07.123.
[23] M.M. Farid, F.A. Hamad, M. Abu-Arabi, Melting and solidification in multidimensional geometry and presence of more than one interface, Energ. Conver. Manage. 39 (1998) 809–818.
[24] P. Lamberg, R. Lehtiniemi, A.M. Henell, Numerical and experimental investigation of melting and freezing processes in phase change material storage, Int. J. Therm. Sci. 43 (2004) 277–287, https://doi.org/10.1016/j.ijthermalsci.2003.07.001.
[25] C. Cárdenas-Ramírez, F. Jaramillo, M.A.G. Botero, Systematic review of encapsulation and shape-stabilization of phase change materials, Journal of Energy Storage 30 (2020) 101495, https://doi.org/10.1016/j.est.2020.101495.
[26] A. Barba, M. Spiga, Discharge mode for encapsulated PCMs in storage tanks, Sol. Energy 74 (2003) 141–148, https://doi.org/10.1016/S0038-092X(03)00117-8.
[27] Q.Q.Q. Al-Yasiri, M. Szabó, Thermal performance of concrete bricks based phase change material encapsulated by various aluminium containers: an experimental study under Iraqi hot climate conditions, J. Energy Storage 40 (2021) 102710, https://doi.org/10.1016/J.EST.2021.102710.
[28] K.A.R. Ismail, R.I.R. Moraes, A numerical and experimental investigation of different containers and PCM options for cold storage modular units for domestic applications, Int. J. Heat Mass Transf. 52 (2009) 4195–4202, https://doi.org/10.1016/J.IJHEATMASSTRANSFER.2009.04.031.
[29] P. Moreno, A. Castell, C. Solé, G. Zsembinszki, L.F. Cabeza, PCM thermal energy storage tanks in heat pump system for space cooling, Energ. Buildings 82 (2014) 399–405, https://doi.org/10.1016/J.ENBUILD.2014.07.044.
[30] A. Heinz, C. Moser, Numerical modelling and experimental testing of a thermal storage system with non-spherical macro-encapsulated phase change material modules, J. Energy Storage 58 (2023) 106427, https://doi.org/10.1016/J.EST.2022.106427.
[31] O.A. Rehman, V. Palomba, D. Verez, E. Borri, A. Frazzica, V. Brancato, T. Botargues, Z. Ure, L.F. Cabeza, Experimental evaluation of different macro-encapsulation designs for PCM storages for cooling applications, Journal of Energy Storage 74 (2023) 109359, https://doi.org/10.1016/j.est.2023.109359.
[32] www.puretemp.com (last access on April 10 2025).
[33] L. Mongibello, N. Bianco, M. Caliano, G. Graditi, Influence of heat dumping on the operation of residential micro-CHP system, Appl. Energy 160 (2015) 206, https://doi.org/10.1016/j.apenergy.2015.09.045.
[34] C. Ji, Z. Qin, S. Dubey, F.H. Choo, F. Duan, Three-dimensional transient numerical study on latent heat thermal storage for waste heat recovery from a low temperature gas flow, Appl. Energy 205 (2017) 1–12, https://doi.org/10.1016/j.apenergy.2017.07.101.
[35] M. Caliano, N. Bianco, G. Graditi, L. Mongibello, Analysis of a phase change material-based unit and of an aluminum foam/phase change material composite-based unit for cold thermal energy storage by numerical simulation, Appl. Energy 256 (2019) 256, https://doi.org/10.1016/j.apenergy.2019.113921.
[36] N. Hu, Z.R. Li, Z.W. Xu, L.W. Fan, Rapid charging for latent heat thermal energy storage: a state-of-the-art review of close-contact melting, Renew. Sustain. Energy Rev. 155 (2022) 11191, https://doi.org/10.1016/j.rser.2021.111918.
[37] C.J. Pan, J. Charles, N. Vermaak, C. Romero, S. Neti, Y. Zheng, Experimental, numerical and analytic study of unconstrained melting in a vertical cylinder with a focus on mushy region effects, Int J Heat Mass Tran 124 (2018) 1015–1024.